

Exploring an innovative method for the automatic recognition of cortical sulci in cranial endocasts

Submitted by: Edwin John de Jager

A dissertation submitted to the Department of Anatomy, School of Medicine, Faculty of Health Sciences, University of Pretoria, in the partial fulfilment of the requirements for the degree:

MSc in Anatomy

Pretoria 2019

Supervisor: Dr Amélie Beudet ^{1,2}

Co-supervisor: Prof Albert-Neels van Schoor¹

¹ Department of Anatomy, Faculty of Health Sciences, University of Pretoria

² School of Geography, Archaeology and Environmental Studies, University of the Witwatersrand

Declaration

I, _____, declare that this thesis is my own work. It is being submitted for the degree of MSc in Anatomy at the University of Pretoria. It has not been submitted before for any other degree or examination at this or any other Institution.

Signed: _____

This _____ day of _____, 2019

Acknowledgements

I am truly grateful to everyone who contributed to helping me ensure the success of this study, I have learnt so much in this time, in many more ways than one.

Thank you from the bottom of my heart to both my supervisors, Dr Amélie Beudet and Prof Albert van Schoor for all the long hours of hard work and effort that they invested in me. Their support and guidance, and even life mentorship over the years gave me the confidence to undertake this project, all of which has found an irreplaceable place in my heart and mind.

A heartfelt thanks to the University of Pretoria for allowing me the opportunity to utilise their facilities in order to perform my research, and to Prof Girdler-Brown from SHSPH, for his statistical advice at the start of this project. Thank you too, to the friends and colleagues at Department of Anatomy for the unconditional help and advice over the years.

I would like to express my sincere thanks to the families of the body donors who graciously supported the academic furtherment of our anatomical scientific endeavours. The opportunity to study the human body throughout my academic career thus far, and the opportunity to engage with the donated specimens used in this project would not have been possible without these individuals.

To Ms G Kruger for access to the outstandingly well-curated Pretoria Bone Collection, and to Dr F de Beer and team, Mr J Hoffman and Dr L Bam, at Necsa for their invaluable input that ensured the realisation of this project through their impeccable attention to detail during the scanning of our specimens. Your expertise surely made this project achievable.

Thank you, sincerely, to Dr E Gillisen, curator at the Royal Museum of Central Africa, Belgium, for allowing us to use their collection for the realisation of our research project.

Prof A Oettlé: thank you for your continued faith in me. It is a true honour for me to have been one of your students, as without this inception, I would have not had the opportunity

to grow with the technological advancements of science and the amazing opportunities that have come with it.

Thank you very much to the National Research Foundation of South Africa for the DST|NRF bursaries (112186 and 116417) that saw me through to completion of my Masters' degree.

Thank you to AESOP+ for financially and administratively enabling me to experience a six-month exchange opportunity in Toulouse, France, and a special thanks to the team at Université Paul Sabatier, Dr Caroline Fontal, Dr Muriel Mescam, Dr Laurent Risser, and everyone from CerCo whom I had the privilege of calling a colleague and friend. Thank you *all* for taking care of me and making me feel at home in the time I spent so far away from my own home, and for reinforcing my interest in Neuroscience. Your hospitality and exposure to the bigger picture of research throughout my France experience will never be forgotten.

A sincere thanks to AMIS, with special acknowledgement to Dr J Dumoncel for his patience and technical expertise that he kindly provided throughout my Masters' project, and his continuing efforts in the larger project that my results played a role in.

To the family at the Faculty of Health Sciences Research Office that Robyn and I were adopted into over the last few years, thank you for all your support, love and encouragement that truly saw us through our enrolment in a Masters' program. You patiently humoured us in all our questions; and showed us the positive impact of true research support.

To the colleagues and friends who stuck with me during my research endeavours, and to those whom I had the honour of meeting while on this journey, thank you all for shaping these last few years into what it became for me.

Lastly, but certainly not least, thank you to my parents, families and my best friend and partner Robyn for always believing in me and supporting me and enabling me to be the best I can be.

Contents

Declaration.....	ii
Acknowledgements.....	iii
List of Figures	viii
List of Tables	xii
List of Appendices	xiii
List of Abbreviations	xv
Abstract.....	18
Keywords:.....	19
Chapter 1: Introduction	20
Chapter 2: Literature review.....	22
2.1 Human sulcal anatomy.....	22
2.1.1 Cortical folding.....	22
2.1.2 Lobes and landmarks	23
2.1.3 The frontal lobe	24
2.1.4 The parietal lobe.....	25
2.1.5 The temporal lobe	26
2.1.6 The occipital lobe.....	27
2.2 Comparative <i>Pan</i> sulcal anatomy.....	28
2.2.1 The frontal lobe	29
2.2.2 The parietal lobe.....	29
2.2.3 The temporal lobe	30
2.2.4 The occipital lobe.....	30
2.3 Human brain evolution: tracking hidden evidence.....	31
2.3.1 Endocasts.....	32
2.4 Application of 3D imaging techniques to endocasts.....	35

2.5 Multimodal brain atlases	36
2.6 Aim:	38
2.7 Objectives:.....	38
Chapter 3: Materials and Methods.....	39
3.1 Study Design	39
3.2 Setting	39
3.3 Sample Population	40
3.4 Exclusion criteria	41
3.5 Equipment/Software	41
3.6 Procedure	43
3.6.1 Formalin-fixed brains:.....	43
3.6.2 Endocasts:.....	43
3.7 Observations	48
3.8 Statistical analysis.....	49
Chapter 4: Results	50
4.1 Extant human brain	50
4.2 Extant human endocasts	55
4.2.1 Frontal lobes	56
4.2.2 Parietal lobes	57
4.2.3 Occipital lobes	57
4.2.4 Temporal lobes	57
4.2.5 Left vs. Right hemisphere	59
4.2.6 Male vs. Female	59
4.3 <i>Pan</i> (Chimpanzee/Bonobo)	62
4.3.1 Frontal lobe.....	62
4.3.2 Parietal lobe:.....	63

4.3.3 Occipital lobe:.....	63
4.3.4 Temporal lobe:.....	63
4.4 Probability Map.....	65
Chapter 5: Discussion.....	72
5.1 Sulcal pattern variation in extant human endocasts	72
5.2 Sulcal pattern impressions on the endocast of <i>Pan</i>	75
5.3 Implications for palaeoneurological studies	77
5.4 The endocast of StW 573 (“Little Foot”)	79
5.5 Limitations.....	80
Chapter 6: Conclusion.....	81
Reference list	82

List of Figures

Figure 2.1: Division of the brain into lobes: F: Frontal lobe, P: Parietal lobe, T: Temporal lobe, O: Occipital lobe; Relevant landmarks: S: Sylvian fissure, c: central sulcus, po: parieto-occipital sulcus, pon: preoccipital notch	24
Figure 2.2: Illustration of sulci commonly described on the superior-lateral surface of human brain. c=central sulcus; fi=inferior frontal sulcus; fm= middle frontal sulcus; fs=superior frontal sulcus; ip=intraparietal sulcus; pc=precentral sulcus; pt=postcentral sulcus; ti=inferior temporal sulcus; ts=superior temporal sulcus.....	26
Figure 2.3: Illustration of occipital sulci, described by Alves et al. (2012). ip=intraparietal sulcus; locs=lateral occipital sulcus; otr=transverse occipital sulcus.....	27
Figure 2.4: Illustration by Connolly (1950) showing the superior lateral surface of a chimpanzee brain showing: S: Sylvian fissure, c: central sulcus, pcs: superior segment of precentral sulcus, pci: inferior segment of precentral sulcus, h: horizontal sulcus, r: sulcus rectus, fs: superior frontal sulcus, fo: fronto-orbital sulcus, pts: superior segment of postcentral sulcus, pti: inferior segment of postcentral sulcus, ip: intraparietal sulcus, ts: superior temporal sulcus, ti: inferior temporal sulcus, L: lunate sulcus, oci: inferior occipital sulci, lc: lateral calcarine sulcus	30
Figure 2.5: A plaster of Paris replica of the Taung child natural endocast by Holloway (1970). See image from Holloway (2004)	32
Figure 2.6: Extant human endocast generated from medical grade CT's (left) compared with an extant human endocast generated from micro CT's (right)	36
Figure 3.1: Screenshot of the custom script used in Matlab to label curves representing sulci and delete unwanted artefacts (Beaudet et al., 2016a)	42
Figure 3.2: Summary of procedure followed for endocasts	44

Figure 3.3: Automatic extraction of an extant human endocast using Endex (A). Resulting endocast mesh (B). Application of crest line detection algorithm (C). Endocast after cleaning of crest lines and labelling (D) (de Jager et al., 2019).....45

Figure 3.4: Summary of process followed in 3.6.2.1 and 3.6.2.2. A: The average surface was calculated by deforming all the endocasts towards the Karcher mean (\bar{x}) of all images in sample; B: Calculate the deformation (where ϕ represents an endocast-specific value) value for each endocast. C: Project all curves (sulci) to common template using ϕ ; D: Variance (σ^2) of each imprint on the endocast can be calculated.....47

Figure 4.1: Sulcal imprints observed on the left hemisphere of twenty individuals. ar=ascending ramus, c=central, d=diagonal, W=fronto-marginal, fo=fronto-orbital, hr=anterior horizontal ramus, if=inferior frontal, ip=intraparietal, it=inferior temporal, L=Lunate, lc=lateral calcarine, fm=middle frontal, o=orbital, oci= lateral/inferior occipital, otr=transverse occipital, pc=precentral, pt=postcentral, rc=retro-calcarine, S=Sylvian fissure, sf=superior frontal, st=superior temporal (de Jager et al., 2019)58

Figure 4.2: Sulcal imprints observed on the right hemisphere of twenty individuals. ar=ascending ramus, c=central, d=diagonal, W=fronto-marginal, fo=fronto-orbital, hr=anterior horizontal ramus, if=inferior frontal, ip=intraparietal, it=inferior temporal, L=Lunate, lc=lateral calcarine, fm=middle frontal, o=orbital, oci=lateral/inferior occipital, oct=occipitotemporal, otr=transverse occipital, pc=precentral, pt=postcentral, rc=retro-calcarine, rh=rhinal, S=Sylvian fissure, sf=superior frontal, st=superior temporal (de Jager et al., 2019).....60

Figure 4.3: Frequency of sulci observed in the left and right hemispheres of human endocasts (de Jager et al., 2019)61

Figure 4.4: Frequency of sulci observed in male and female human endocasts (de Jager et al., 2019).....61

Figure 4.5: Frequency of sulcal imprints observed on six chimpanzee endocasts.....62

Figure 4.6: Sulcal pattern variation on six chimpanzee endocranial casts. A: Pan; B: Pan; C: Pan; D: Pan; E: Pan; F: Pan. The following sulci were identified: W=fronto-marginal sulcus; fo=fronto-orbital sulcus; r=sulcus rectus; fs=superior frontal sulcus; fm=middle frontal sulcus; fi=inferior frontal sulcus; d=diagonal sulcus; pc=precentral sulcus; h=horizontal ramus of pci; c=central sulcus; pt=postcentral sulcus; S=Sylvian fissure; ts=superior temporal sulcus; tm=middle temporal sulcus; ip=intraparietal sulcus; pl=pre-lunate sulci; L=lunate sulcus; oci=inferior occipital sulcus; lc=lateral calcarine sulcus ..64

Figure 4.7: Key – dark red indicates mean (\bar{x}); light blue/white indicates variations up to two standard deviations (std dev.) from the mean66

Figure 4.8: Probability map for the fronto-marginal-, fronto-orbital-, superior frontal- and middle frontal sulci on the left and right hemispheres.....67

Figure 4.9: Probability map for the inferior frontal-, precentral-, central- and postcentral sulci on the left and right hemispheres.....68

Figure 4.10: Probability map for the intraparietal-, transverse occipital-, lunate- and lateral/inferior occipital sulci on the left and right hemispheres69

Figure 4.11: Probability map for the lateral calcarine-, retro-calcarine-, superior temporal- and inferior temporal sulci on the left and right hemispheres.....70

Figure 4.12: Probability map for the Sylvian fissure, anterior horizontal ramus, ascending ramus and diagonal sulcus on the left and right hemispheres71

Figure 5.1: Illustration of the distribution of the imprints formed by superior frontal sulcus (yellow); the middle frontal sulcus (pink) and the fronto-marginal sulcus (red) on the frontal lobe73

Figure 5.2: Illustration showing the probability map of the impressions formed by the precentral sulcus (green); the central sulcus (yellow) and the postcentral sulcus (orange) on the left and right hemispheres.....74

Figure 5.3: Illustration of sulci identified on the left occipital lobe of one Pan cranial endocast76

Figure 5.4: Photograph of macaque (*macaca fuscata*) brain from Minh and Hamada (2017); pr=principal sulcus/sulcus rectus; ar=arcuate sulcus/inferior precentral sulcus; sy=Sylvian fissure; st=superior temporal sulcus; ce=central sulcus; ip=intraparietal sulcus; lu=lunate sulcus.....78

List of Tables

Table 2.1: A summary of the five "levels" of data that can be collected from endocasts. Adapted from Holloway (1978).....	33
Table 3.1: Summary of all samples collected.....	40
Table 4.1: Summary of sulci observed on each hemisphere of the frontal lobe	50
Table 4.2: Summary observations for the Sylvian fissure on each hemisphere.....	52
Table 4.3: Summary observations for the central sulcus on each hemisphere	52
Table 4.4: Summarising sulci observed on each hemisphere of the parietal lobe.....	53
Table 4.5: Summary sulci observed on each hemisphere on the occipital lobe	53
Table 4.6: Summarising sulci observed on each hemisphere on the temporal lobe	54
Table 4.7: Frequency of sulci observed for left and right hemispheres in humans (de Jager et al., 2019).....	55

List of Appendices

Appendix A: Faculty of Health Sciences Research Ethics Committee, UP (certificate no. 339/2017)	91
Appendix B: Permission letter for access to the non-human primate collection at the Royal Museum of Central Africa, Belgium	92
Appendix C: Formalin-fixed human brain demographics after exclusions were made	93
Appendix D: Extant human endocast demographics after exclusions were made	93
Appendix E: <i>Pan</i> endocast demographics after exclusions were made	93
Appendix F: Examples of sulcal patterns observed on formalin-fixed human brains	94
Appendix G: Hand drawn notes of sulcal patterns observed on the occipital lobes of formalin-fixed human brains	95
Appendix H: De Jager EJ, van Schoor AN, Hoffman JW, Oettlé AC, Fonta C, Mescam M, Risser L, Beaudet A (2019) Sulcal pattern variation in extant human endocasts. <i>Journal of Anatomy</i> 235:803–810. doi: 10.1111/joa.13030	96
Appendix I: Poster → De Jager EJ, Van Schoor AN, Hoffman JW, Oettle AC, Fonta C, Beaudet A (2018) Sulcal pattern variation in extant human endocasts. In: <i>American Journal of Physical Anthropology: 87Th Annual Meeting of the American Association of Physical Anthropologists, Austin; pp. 63-63</i>	96
Appendix J: Abstract of oral presentation presented at the 47 th annual conference of the Anatomical Society of Southern Africa	97
Appendix K: URL to → Beaudet A, Clarke RJ, de Jager EJ, Bruxelles L, Carlson KJ, Crompton R, de Beer F, Dhaene J, Heaton JL, Jakata K, Jashashvili T, Kuman K, McClymont J, Pickering TR, Stratford D (2019) The endocast of StW 573 (“Little Foot”) and hominin brain	

evolution. *Journal of Human Evolution* 126:112–123. doi: 10.1016/j.jhevol.2018.11.009

.....98

Appendix L: Poster → Dumoncel J, Subsol G, Durrleman S, Oettlé AC, Lockhat Z, Suleman FE,

de Jager EJ, Beaudet A (2018) A quantitative comparison of the brain and the inner

surface of the cranium. In: 10ème Symposium de Morphométrie et Évolution des

Formes. Bordeaux98

List of Abbreviations

General abbreviations	
Abbreviation	Definition
\bar{x}	Mean
μm	Micrometres
ϕ	Phi – used to denote the displacement field
σ^2	Variance
AESOP+	A European and South African Partnership on Heritage and Past+
AMIS	Anthropobiologie Moléculaire et d’Imagerie de Synthèse
CerCo	Centre de Recherche Cerveau & Cognition
CSF	Cerebrospinal fluid
CT	Computed Tomography
EEG	Electroencephalogram
F	Female
fMRI	Functional Magnetic Resonance Imaging
LH	Left hemisphere
M	Male
Micro-CT or micro-CT	Microfocus X-ray Computed Tomography
MIXRAD	Micro-focus X-ray Radiography and Tomography facility
mya	Million years ago
MRI	Magnetic Resonance Imaging
Necsa	Nuclear Energy Corporation of South Africa
NRF	National Research Foundation
obj	Object (Wavefront) – an image file format
RH	Right hemisphere
SPAM	Statistical/Probabilistic Anatomy Maps
TIFF	Tagged Image File Format

UGCT	Centre for X-ray Tomography of the Ghent University
UP	University of Pretoria
UPS	Université Paul Sabatier
vtk	Virtual tool kit – an image file format

Sulci abbreviations (adapted from Connolly, 1950)	
Abbreviation	Definition
a	Ramus of superior temporal sulcus
ar	Ascending ramus of Sylvian fissure
c	Central sulcus
d	Diagonal sulcus
h	Horizontal ramus of inferior precentral sulcus
hr	Horizontal ramus of Sylvian fissure
fi	Inferior frontal sulcus
fm	Middle/intermediate frontal sulcus
fo	Fronto-orbital sulcus
fs	Superior frontal sulcus
ip	Intraparietal sulcus
L	Lunate sulcus
lc	Lateral calcarine sulcus
o	Orbital sulci
oci	Inferior occipital sulcus some cases referred to as lateral/inferior occipital sulcus
otr	Transverse occipital sulcus
pc	Precentral sulcus
pci	Inferior precentral sulcus
pcs	Superior precentral sulcus

pcm	Middle precentral sulcus
pl	Prelunate sulci
pt	Postcentral sulcus
pti	Inferior postcentral sulcus
ptm	Middle postcentral sulcus
pts	Inferior postcentral sulcus
r	Sulcus rectus
rc	Retro-calcarine sulcus
S	Sylvian/Lateral fissure
sca	Anterior subcentral sulcus
scp	Posterior subcentral sulcus
ti	Inferior temporal sulcus
tm	Middle temporal sulcus
ts	Superior temporal sulcus
W	Fronto-marginal sulcus

Abstract

Knowledge of human brain evolution primarily relies on the interpretation of palaeoneurological evidence. In the absence of any direct evidence of the fossil neural condition, an endocast (i.e., replica of the internal table of the bony brain case) would constitute a proxy for reconstructing a timeline and mode of cerebral changes in human evolution. The identification of cerebral imprints, and more particularly, of cortical sulci, is indeed critical for assessing the topographic extension and structural organisation of cortical areas. As demonstrated by historical debates in palaeoneurology, however, the description of these crucial landmarks in fossil endocasts is challenging. The recent introduction of high-resolution imaging techniques in (palaeo)neurology offers new opportunities for tracking detailed endocranial neural characteristics. In such context, this study aimed to provide an atlas documenting the variation in the extant human, common chimpanzee and bonobo endocranial sulcal patterns for subsequent use as a comparative platform for the study of the fossil record. The total brain sample population for this study consisted of 60 formalin-fixed human brains from the Department of Anatomy, University of Pretoria, South Africa. Additionally, 58 extant human dry crania from the Pretoria Bone Collection (University of Pretoria, South Africa) which were detailed previously by X-ray microtomography (micro-CT) at the MIXRAD facility, located at the South African Nuclear Corporation (Necsa), Pelindaba, and 22 common chimpanzee and bonobo crania from the Royal Museum for Central Africa (Tervuren, Belgium) that had also been detailed previously using micro-CT at the Centre for X-ray Tomography of the Ghent University (UGCT) were processed and evaluated for inclusion in the study population. Sulci on formalin-fixed brains were documented to create a database of sulcal patterns representing a South African brain sample population. The endocasts were analysed using various software programs and appropriate algorithms, during the post-acquisition process. Finally, a probability map was constructed to document the variation of sulcal imprints on extant human endocasts, based on the identified sulci. This semi-automatic method provides an innovative, non-invasive, observer-independent method to investigate human endocranial structural organisation and a promising perspective for discussing long-standing questions in palaeoneurology.

Keywords:

sulci detection; brain cast; cerebral variation; human neuroanatomy; palaeoneurology

Chapter 1: Introduction

Since brains are not preserved in the fossil record, palaeoneurologists are presented with the challenge of relying on the inner surface of the braincase to reconstruct the human brain evolutionary history. For this reason, researchers made use of endocasts to infer basic conclusions on brain size, shape and general surface morphology (Falk, 1980a, 1987, 2014; Holloway, 1978; Holloway *et al.*, 2004). In addition to the direct description of fossil endocasts that have been attributed to humans' relatives, comparative anatomy involving representatives of *Homo* (i.e., humans) and *Pan* (i.e., common chimpanzees and bonobos) is considered crucial for inferring evidence of cerebral changes in the human lineage and tracking the earliest evidence of human-like features in the fossil record. Indeed, common chimpanzees and bonobos – humans' closest living relatives – are usually considered as a proxy for estimating the ancestral hominin condition (de Sousa and Cunha, 2012).

These endocasts, as do other tools used in palaeoneurology, have limitations when dealing with the fossil record. Firstly, information is limited to the external cortical surface and nothing can be inferred about the subcortical structures. Moreover, fossil crania are often severely damaged and may be incomplete or distorted due to taphonomic processes; thereby providing only partial endocasts. Other limitations reported include the inaccurate reproduction of cerebral details on the endocranial surface due to the presence of intracranial components (e.g., arterial supply of the brain, cerebrospinal fluid, and meningeal membranes) (Neubauer, 2014). Furthermore, the sulcal pattern in the extant¹ human brain is also known to be highly variable (Connolly, 1950; Ono *et al.*, 1990; Ribas, 2010) and early descriptions of these patterns in fossil endocasts mostly relied on visual inspection and palpation of the endocranial surface (Falk, 1980a, 1980b, 1983; Holloway, 1981). Most of the uncertainties in human palaeoneurology have resulted from these limitations; which have contributed to long-standing debates, such as the identification of the lunate sulcus in the endocast of the Taung child (*Australopithecus africanus*) and how its descriptions may present potential similarities to either a human-like or chimpanzee-like pattern (Holloway, 2008). In

¹ **extant** – “still standing”; “taxa that are alive today” (Wood, 2015)

this context, it may be tempting to suggest that correct interpretation of details on the endocranial surface almost always relies on the neuroanatomical knowledge of the researcher (Zollikofer and Ponce de León, 2013).

Technological advances in medical imaging techniques have potentially enabled palaeoneurologists to deal with some of these limitations: endocasts of even the most fragmented fossil cranial vaults can now be virtually extracted, reconstructed and interpreted without damaging the specimen (Spoor *et al.*, 2000; Gunz *et al.*, 2010; Neubauer *et al.*, 2012; Zollikofer and Ponce de Leon, 2013; Neubauer, 2014; Spoor *et al.*, 2015). Holloway (1980) published one of the first attempts to quantitatively assess regional differences in a brain endocast. Since then, however, little has been done to improve knowledge of the cerebral organisation in fossil species. Current applications of imaging techniques in palaeoneurology are, however, relatively limited and unexplored when compared to medical studies. For instance, population-based brain atlases – an extensive database of brain images of living patients – have long been the focus of study in clinical fields. These atlases retain information pertaining to intrapopulation brain variations, proving useful in the detection of pathology in patients and assistive in functional image analysis (Thompson *et al.*, 2000; Toga and Thompson, 2001) and revealing previously unreported fascinating aspects of the human brain (Glasser *et al.*, 2016). To the best of our knowledge, this kind of approach has not been applied in a paleoanthropological context yet.

This study therefore intended to integrate the concept of a modern human brain atlas with cranial endocasts to establish an extensive reference database of virtual endocranial cortical surface variations in extant *Homo* and *Pan*; thereby improving the accuracy of cortical sulci and gyri imprint detection and identification on fossil endocasts.

Chapter 2: Literature review

2.1 Human sulcal anatomy

For the purpose of this study (sections [2.6](#) - [2.7](#)) this literature review will focus on the sulci visible on the superolateral surface of the brain and some additional sulci that potentially imprint on the inner table of the cranial vault.

2.1.1 Cortical folding

During the fifth week of human embryonic development, the cerebral hemispheres of the brain develop as bilateral outpocketings from the prosencephalon of the forebrain (Sadler and Langman, 2012). Each hemisphere has three surfaces (medial, superolateral and inferior) that are riddled with intricate, erratic patterns of convoluted folds, otherwise known as gyri, that are separated by shallow furrows, known as sulci; or deep furrows, known as fissures. The formation of sulci and gyri follows a specific sequence. Primary sulci are first visualised as grooves in specific brain regions, secondary branches then develop from the primary sulci, which are followed by tertiary branches. First to form is the longitudinal fissure (Gestational week: 8-22), separating the two cerebral hemispheres. Primary sulci, namely the Sylvian (lateral fissure), Cingulate, Parieto-occipital and Calcarine (Gestational week: 14-16); Central and Superior Temporal (Gestational week: 20-24); and Superior Frontal, Postcentral, and Intraparietal (Gestational week: 25-26) are responsible for the subdivision of the hemispheres into the frontal, parietal, occipital and temporal lobes; which were named after, and closely resemble the inner surface(s) of their overlying cranial bones (Bosman, 2008; Standring *et al.*, 2008). Secondary sulci (Gestational week: 30-35) and tertiary sulci (Gestational week: 36) follow in development well into the postnatal period (Stiles and Jernigan, 2010). Despite a paucity of information pertaining to cortical folding, various innovative methods are being explored to study the process of gyrification during brain development (Tallinen *et al.*, 2016; Garcia *et al.*, 2018).

2.1.2 Lobes and landmarks

The lateral and basal surfaces of the cerebral hemisphere are visibly lined by a deep channel referred to as the lateral fissure of Sylvius (from here on will be referred to as the Sylvian fissure), which forms the major separation between the frontal and parietal lobes above, from the temporal lobe below (Fig. 2.1). On the lateral surface, the Sylvian fissure is usually divided into three segments: the anterior segment, that divides into the short anterior horizontal ramus rostrally and the anterior ascending ramus caudally (a feature unique to extant human brains); the horizontally-orientated middle segment; and the posterior segment, which terminates vertically (Ono *et al.*, 1990; Duvernoy *et al.*, 1999).

The central sulcus (fissure of Rolando) starts on the upper margin of the brain where it usually has a hook-like extension (notch) on the medial surface of the brain, immediately behind the midpoint between the frontal- and occipital pole (Fig. 2.1) after which it follows an oblique course inferiorly on the lateral surface. The inferior end of the central sulcus is typically separated from the Sylvian fissure by the subcentral gyrus (Ono *et al.*, 1990; Duvernoy *et al.*, 1999). The central sulcus marks the boundary between the frontal and parietal lobe and defines the primary motor and somatosensory areas of the cortex, located in the precentral and postcentral gyri, respectively (Standring *et al.*, 2008; Petrides and Pandya, 2011). Amunts *et al.* (1996, 2000) reported that the central sulcus depth may correlate with handedness and sex.

The calcarine and parieto-occipital sulci can be seen on the posterior region of the medial surface. The parieto-occipital sulcus originates on the superomedial boundary of the cerebral hemisphere and runs obliquely anteriorly, until it meets the calcarine sulcus. On the superolateral surface, the junctions between the parietal and occipital lobes and those between the temporal and occipital lobes are indicated by an imaginary line drawn from the origin of the parieto-occipital sulcus (seen as a notch on the upper margin of the hemisphere), on the superolateral margin to the preoccipital notch (Fig. 2.1). The majority of the calcarine sulcus is limited to the medial surface and is divided into three parts, joining with the parieto-occipital sulcus at the corpus callosum. The visual cortex lies above and below the posterior part of the calcarine sulcus (Ono *et al.*, 1990; Duvernoy *et al.*, 1999; Standring *et al.*, 2008).

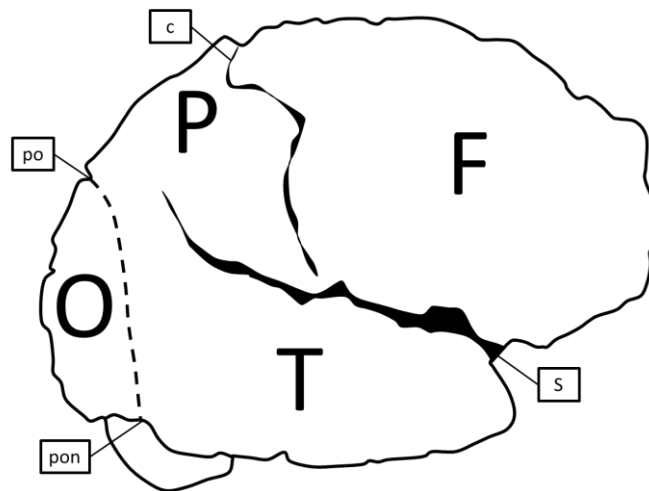


Figure 2.1: Division of the brain into lobes: F: Frontal lobe, P: Parietal lobe, T: Temporal lobe, O: Occipital lobe; Relevant landmarks: S: Sylvian fissure, c: central sulcus, po: parieto-occipital sulcus, pon: preoccipital notch

2.1.3 The frontal lobe

The precentral gyrus lies against the central sulcus on the superolateral surface and extends onto the medial surface. The gyrus mainly comprises the primary motor cortex (Brodmann's area 4) and a partial area of the premotor cortex (Brodmann's area 6). Anteriorly, the precentral gyrus is limited by the precentral sulcus, which is typically divided into an inferior-, middle/intermediate-, superior- and marginal/medial precentral sulcus (Fig. 2.2). Anterior to the precentral sulcus the frontal lobe is divided into a superior, middle and inferior frontal gyrus by the superior and inferior frontal sulci, respectively, which generally originates from the superior and inferior segments of the precentral sulcus, respectively (Fig. 2.2). The superior frontal gyrus can be riddled with multiple sulci that Ono *et al.* (1990) referred to as the medial frontal sulci. The middle frontal gyrus is occupied by the middle/intermediate frontal sulcus, known to connect with the fronto-marginal sulcus on the rostral border of the frontal lobe (Fig. 2.2) (Petrides *et al.*, 2011). In a perfect/ideal specimen the inferior frontal gyrus is invaded by the diagonal sulcus posteriorly, which delineates the opercular part of the inferior frontal gyrus, directly anterior to it the ascending ramus of the Sylvian fissure, which together with the anterior horizontal ramus of the Sylvian fissure, forms the borders of the triangular part of the inferior frontal gyrus. The cortical areas (Brodmann's areas 44 and 45), found in the opercular and triangular parts, comprise Broca's motor speech area. Most rostrally on the inferior frontal gyrus, authors have identified the fronto-orbital sulcus (see

Ono *et al.*, 1990) or the lateral part of the fronto-marginal sulcus (see Connolly, 1950). The variations in naming these sulci are mainly a result of misidentification or opinion differences amongst authors. The orbital region of the frontal lobe lies above the orbital plate of the frontal bone. Studies have shown that the orbitofrontal surface has four major sulci forming a common pattern representing an “H,” “K,” or an “X”. The olfactory sulcus crosses the orbital part of the frontal lobe on its medial margin, overlaid by the olfactory bulb and tract. Medial to the olfactory sulcus, the gyrus rectus can be seen (Connolly, 1950; Ono *et al.*, 1990; Duvernoy *et al.*, 1999; Chiavaras and Petrides, 2000; Standring *et al.*, 2008; Petrides and Pandya, 2011).

2.1.4 The parietal lobe

The lateral surface of the parietal lobe is divided into three by the intraparietal and postcentral sulci. The postcentral sulcus, directly posterior to the central sulcus, ends inferiorly just above the posterior ramus of the lateral fissure (Fig. 2.2). The postcentral gyrus, containing the primary somatosensory cortex (Brodmann’s areas 1, 2, 3a and 3b) is situated between the central- and postcentral sulci. The intraparietal sulcus divides the parietal lobe into a superior and an inferior parietal lobule. In most cases the intraparietal sulcus consists of three segments, of which first is the ascending segment (inferior segment of postcentral sulcus). The second part is the horizontal segment, transitory between the ascending segment and the third segment, which is the descending segment. Instances where the descending segment crosses the occipital border is known as the par-occipital sulcus (see Connolly, 1950) or by later authors as the intra-occipital sulcus (see Duvernoy *et al.*, 1999) (Fig. 2.2). The inferior parietal lobule is divided into three parts. The anterior part is moulded around the posterior ramus of the lateral fissure, forming the supramarginal gyrus. The middle part of the lobule moulds around the superior temporal sulcus and is called the angular gyrus. Lastly, the posterior part of the lobule moulds around the posterior end of the inferior temporal sulcus and is continuous with the occipital lobe. Collectively, the supramarginal gyrus, angular gyrus and the posterior end of the superior temporal gyrus with the long transverse temporal gyri (planum temporale) house Wernicke’s auditory association area (Brodmann’s areas 22, 39, 40, 41 and 42) (Connolly, 1950; Ono *et al.*, 1990; Duvernoy *et al.*, 1999; Standring *et al.*, 2008).

2.1.5 The temporal lobe

The temporal lobe's lateral surface is divided into three parallel temporal gyri by the superior and inferior temporal sulci (Fig. 2.2). The superior temporal sulcus (often referred to as the parallel sulcus) is generally divided into an anterior and a posterior segment. The inferior temporal sulcus lies inferior and parallel to the superior temporal sulcus, and generally consists of multiple segments of where the posterior segment is frequently referred to as the anterior occipital sulcus. Brodmann's area 42 (auditory function) can be found on the posterior portion of the superior temporal gyrus, where it joins with the anterior transverse temporal gyrus (Ono *et al.*, 1990; Duvernoy *et al.*, 1999; Standring *et al.*, 2008).

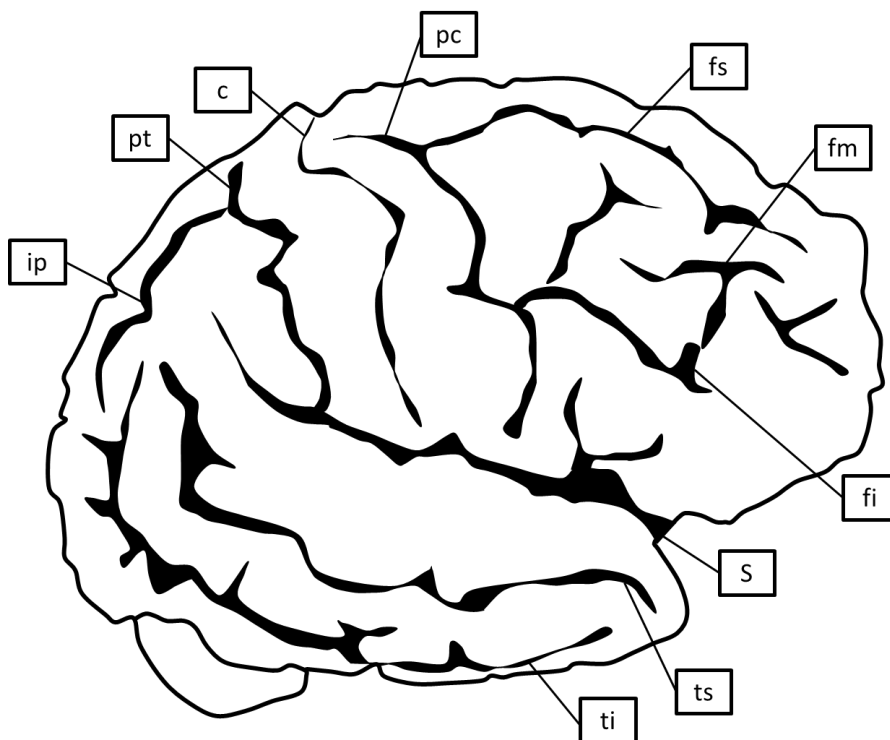


Figure 2.2: Illustration of sulci commonly described on the superior-lateral surface of human brain. S=Sylvian fissure; c=central sulcus; fi=inferior frontal sulcus; fm= middle frontal sulcus; fs=superior frontal sulcus; ip=intraparietal sulcus; pc=precentral sulcus; pt=postcentral sulcus; ti=inferior temporal sulcus; ts=superior temporal sulcus

2.1.6 The occipital lobe

The human occipital sulci are highly complex and variable, where the easiest description involves visualizing the same gyral configuration as that of the frontal lobe (i.e., superior-, middle and inferior occipital gyri). The superior- and middle occipital gyri are separated by the posterior extension of the intraparietal sulcus, which terminates caudally as a horizontally orientated sulcus, called the transverse occipital sulcus (Fig. 2.3). The middle- and inferior occipital gyri are separated by the lateral occipital sulcus, also termed by authors as the inferior occipital sulcus (Fig. 2.3) (Duvernoy *et al.*, 1999; Iaria and Petrides, 2007; Alves *et al.*, 2012). Ono *et al.* (1990) used the terms lateral occipital sulcus and inferior occipital sulcus synonymously to describe up to three sulci on the lateral surface of the occipital lobe.

Occasionally, on the most caudal part of the occipital lobe the posterior extension of the calcarine sulcus, i.e., the retro-calcarine sulcus, can be seen extending over the occipital pole. Connolly (1943) described a lateral calcarine-/external calcarine sulcus that embraces the caudal end of the retro-calcarine sulcus. The descriptions of the lunate sulcus in humans remain to be highly variable among authors (Connolly, 1950; Ono *et al.*, 1990; Duvernoy *et al.*, 1999; but see Allen *et al.*, 2006 and Alves *et al.*, 2012). Allen *et al.*, (2006) reported that the human lunate sulcus is not an independent 'true' lunate sulcus but rather a composite sulcus made up of existing occipital sulci, illustrating a crescent shaped sulcus transgressing much of the occipital lobe.

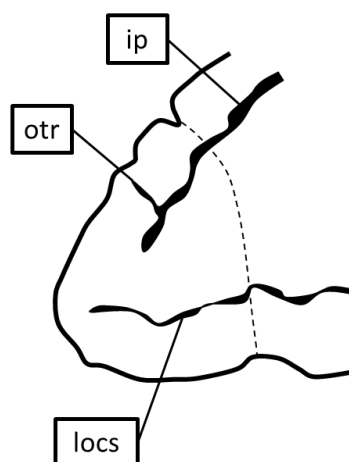


Figure 2.3: Illustration of occipital sulci, described by Alves *et al.* (2012). *ip*=intraparietal sulcus; *locs*=lateral occipital sulcus; *otr*=transverse occipital sulcus

2.2 Comparative *Pan* sulcal anatomy

The genus *Pan* are considered as the closest living relatives of anatomically modern humans; their divergence from the most recent common ancestor of the two tribes was suggested to have occurred more than 8 million years ago by Arnason and Janke (2002) and Langergraber *et al.* (2012). A more recent divergence has been suggested by Prado-Martinez *et al.* (2013) but these findings were later refuted by Moorjani *et al.* (2016) by looking at CpG transitions instead of substitution rates of base pairs, who estimated the divergence to have occurred closer to 12 million years ago. Accordingly, the genus *Pan* (more specifically, the chimpanzee) is considered to represent the ancestral sulcus morphology and would lack the features acquired along the hominin evolutionary history. In order to determine if a certain feature is “primitive” or “derived”, it is important to understand the differences between the sulcal patterns of extant humans and chimpanzees to adequately compare this information with the information acquired from the fossil record (McBrearty and Jablonski, 2005; de Souse and Cunha, 2012).

Two species are acknowledged for the genus *Pan* – *Pan troglodytes* (i.e., common chimpanzees) and *Pan paniscus* (i.e., bonobos). Considerably less convoluted brains are observed in *Pan* compared to that of *Homo*, however, similarities may still be observed. One such example is the Sylvian fissure; which may be observed on the superolateral surface on the brain, dividing the frontal lobe and the temporal lobe (Fig. 2.4). Similarly, the central sulcus can be observed dividing the frontal and parietal lobes more rostrally in chimpanzees, compared to humans (Fig. 2.4). Finally, the superior temporal sulcus generally forms a continuous sulcus transgressing the lateral temporal surface. As in human brains, the occipital lobe and the parietal lobe, as well as the temporal lobe are separated from each other via an imaginary line that can be drawn between the parieto-occipital sulcus and preoccipital notch (Connolly, 1950; Falk *et al.*, 2018).

2.2.1 *The frontal lobe*

The frontal lobe presents with the precentral sulcus. Anterior to the precentral sulcus the frontal lobe divides into a superior, middle, and inferior frontal gyrus by the superior and inferior frontal sulci. The inferior- and middle/intermediate frontal sulci are referred to as phylogenetically “new” sulci due to their exclusive presence in great apes and humans (Fig. 2.4). More specifically, the inferior frontal sulcus is derived from the arcuate-/inferior segment of the precentral sulcus in monkeys. Similarly, the middle frontal sulcus is derived from the sulcus rectus/principal sulcus of monkeys. Its caudal end is usually connected, and derived from, the horizontal branch of the precentral sulcus (referred to as the arcuate sulcus in monkeys). Additional sulci that may be present on the frontal lobe include the fronto-marginal sulcus, fronto-orbital sulcus, sulcus rectus, horizontal branch of precentral sulcus, and the diagonal sulcus. The fronto-orbital sulcus in chimpanzees is closely related to Brodmann’s area 44 and Brodmann’s area 45 (Keller *et al.*, 2009). The fronto-orbital sulcus of chimpanzees is not homologous to the fronto-orbital sulcus identified by Ono *et al.* (1990) in human brains. It is hypothesized that the fronto-orbital sulcus in chimpanzees is the homologue of the anterior limiting sulcus of the insula in humans. Although the orbital surface presents with an orbital sulcus, it appears to be significantly less complex than that of human brains (Fig. 2.4) (Connolly, 1950; Falk *et al.*, 2018).

2.2.2 *The parietal lobe*

As with humans, the parietal lobe exhibits the postcentral sulcus posterior to the central sulcus (Fig. 2.4). The inferior segment of the post central sulcus may be connected with the intraparietal sulcus, dividing the parietal lobe into superior and inferior parietal lobules (Connolly, 1950).

2.2.3 The temporal lobe

The temporal lobe is divided into superior, middle and inferior temporal gyri by the superior and middle temporal sulci (Fig. 2.4) (Connolly, 1950).

2.2.4 The occipital lobe

The occipital lobe in chimpanzees is rostrally delineated by the lunate (Affenspalte) sulcus; which is generally identified as an arch rostral to the obliquely oriented lateral calcarine sulcus. The lunate sulcus in chimpanzees is known to closely demarcate the anterior border of Brodmann's area 17. The lateral calcarine sulcus can be observed dividing the occipital lobe of the chimpanzee brain into a superior and inferior lobe. The inferior occipital sulcus can be seen protruding onto the inferior lobule (Connolly, 1950; Falk *et al.*, 2018).

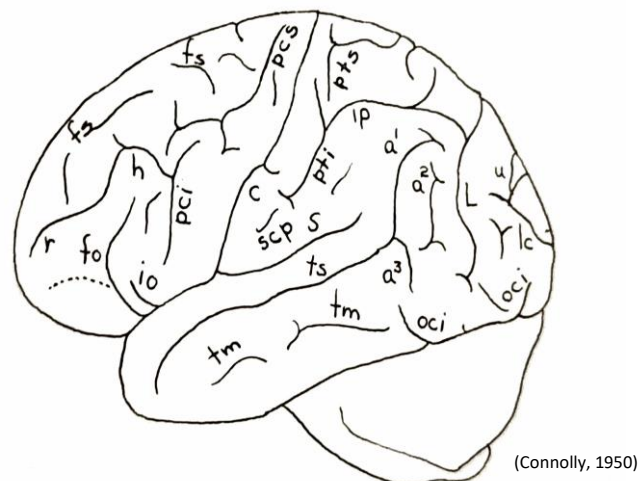


Figure 2.4: Illustration by Connolly (1950) showing the superior lateral surface of a chimpanzee brain showing:
S: Sylvian fissure, c: central sulcus, pcs: superior segment of precentral sulcus, pci: inferior segment of precentral sulcus, h: horizontal sulcus, r: sulcus rectus, fs: superior frontal sulcus, fo: fronto-orbital sulcus, pts: superior segment of postcentral sulcus, pti: inferior segment of postcentral sulcus, ip: intraparietal sulcus, ts: superior temporal sulcus, ti: inferior temporal sulcus, L: lunate sulcus, oci: inferior occipital sulci, lc: lateral calcarine sulcus

2.3 Human brain evolution: tracking hidden evidence

One of the major questions in palaeoneurology concerns the timing and mode of the emergence of *Homo*-like cerebral features in the hominin² fossil record. The South African fossil record currently acknowledges up to six fossil hominin taxa: *Australopithecus africanus*, which was found at Makapansgat, Sterkfontein, and Taung; the hypothesized *Australopithecus prometheus*, found at Makapansgat and Sterkfontein (e.g., “Little foot”); *Australopithecus sediba* – found at Malapa; *Paranthropus robustus* from Kromdraai, Swartkrans and Sterkfontein; and finally, early *Homo* from Swartkrans and Sterkfontein, and *Homo naledi* from Rising Star (Wood and Boyle, 2016; Clarke, 2019). These fossilised remains preserve numerous valuable natural endocasts that continue to play a critical role in palaeoneurological research since the study of the fossil hominin brain acts as a crucial interface between the organism and its environment (Le Gros Clark, 1971).

Despite fossil evidence, some questions pertaining to human brain evolution remain unresolved. For instance, the position of the lunate sulcus on the Taung child endocast (see Fig. 2.5) is still debated, likely due to the poor preservation of cortical features on endocasts. The Taung child debate is centred around the concept of cortical reorganisation in the South African early hominins. Holloway (1981, 2008) suggested that cortical reorganisation occurred prior to cortical expansion and that the Taung child brain subsequently represents a more human-like organisation. Alternatively, Falk (1980b) suggested that cortical reorganisation only happened after the cortex expanded and that the Taung child endocast represents a more “pongid”-like organisation. Such a question is critical in palaeoneurology because tracking the first occurrence of human-like cerebral features in the hominin lineage is fundamental for reconstructing the evolutionary history of the human brain.

² **Hominin** – any species that is more closely related to modern humans than to any other living taxa (Wood, 2015)

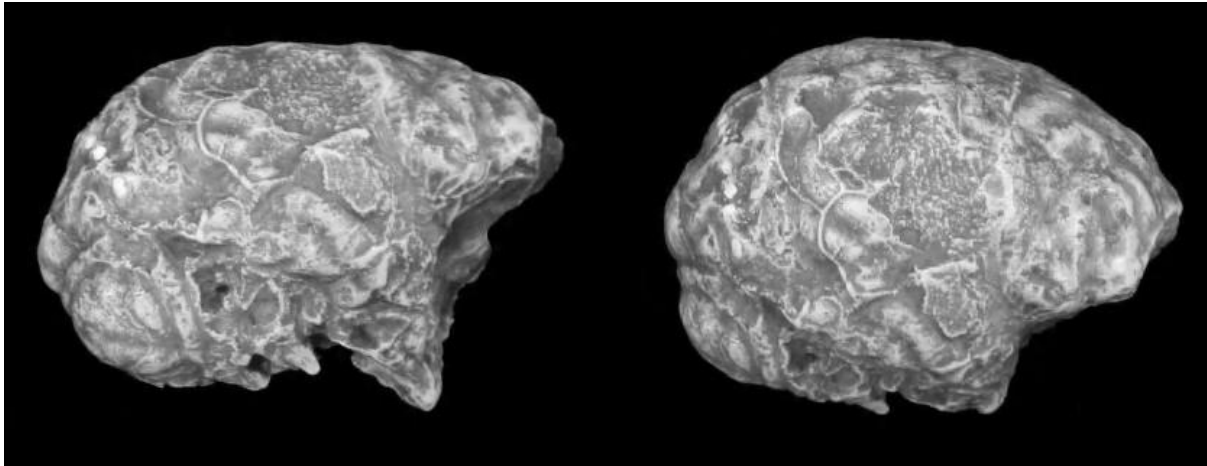


Figure 2.5: A plaster of Paris replica of the Taung child natural endocast by Holloway (1970). See image from Holloway (2004)

2.3.1 Endocasts

Brain endocasts – the only direct evidence of fossil hominin neural condition – are casts representing the inner surface of the cranium: the region of the skull that houses the brain; and could be either natural or artificial (Holloway, 1978; Holloway *et al.*, 2004). Natural, almost “rock-like” endocasts are typically formed when fine sediments infiltrate the cranium of skeletal remains through the cranial foramina. With time, the sediment solidifies when continually exposed to calcareous water e.g., Taung child (*Australopithecus africanus*) endocast, first described by Raymond Dart (1926). Some casts are made using a moulding material (such as liquid latex or silicon) applied to the cranial region of interest (Holloway *et al.*, 2004). Alternatively, plaster-of-Paris may be poured into the cranial portions of interest for casting, however, modern medical imaging techniques have gained popularity for their virtual visualisation capabilities (Holloway *et al.*, 2004; Zollikofer and Ponce de León, 2013).

Since an endocast is not a cast of the brain, but a cast made of the internal table of the cranial bone, the three layers of membranous tissue surrounding the brain: pia mater (closest to the brain), arachnoid mater (surrounds the pia mater and contains cerebrospinal fluid (CSF)) and the tough dura mater (most outer layer that adheres to the internal table of the cranial bone) are important factors to account for when measuring cranial capacity or working with endocasts in general. Other factors that can affect the accuracy of size evaluation is the

completeness of the endocast and presence of distortion of the endocast (Holloway *et al.*, 2004; Zollikofer and Ponce de León, 2013).

Holloway (1978) described at least five “levels” of data that can be obtained from endocasts, depending on their completeness and degree of expression of cortical details (Table 2.1; Holloway, 1978). These levels have since been re-categorised into three types of morphological information: size, shape and structural organisation (Zollikofer and Ponce de León, 2013).

Table 2.1: A summary of the five "levels" of data that can be collected from endocasts. Adapted from Holloway (1978)

Level 1	Gross brain size (i.e. volume of neural mass with dural tissue, ventricles, CSF etc.) <ul style="list-style-type: none"> • Used to calculate neural mass • Used to calculate encephalisation quotient/relative brain size • Can be compared to other biological variables (construct a timeline) • Morphometry (i.e. shape and size relationship between taxa)
Level 2	Areal determination (i.e. division into major lobar regions) <ul style="list-style-type: none"> • Purely qualitative • Dependant on accurate identification of sulcal patterns • Provides information on local asymmetries
Level 3	Major sulcal, gyral and meningeal blood vessel pattern identification <ul style="list-style-type: none"> • Related to level 2 but more specific to sulcal pattern variation over time
Level 4	Identifications of secondary and tertiary sulci and gyri related to functional areas (i.e. Broca's, Wernicke's etc.)
Level 5	Secondary and tertiary convolutions can be related to functional models based on neurophysiological mappings of the cerebral cortex of different animals
Level 6	“Does not really exist” but refers to inferences made on subcortical relationships based on comparative neuroanatomy knowledge

Endocranial size is considered an estimate of brain size. In primates it provides an estimate of body size (see Manger *et al.*, 2013) using the encephalization quotient which was first introduced by Harry Jerison (1973) to account for the allometric effects of body size on brain size (Table 2.1) (Wood, 2015). Although highly debatable, encephalization quotient is considered as an indicator of behavioural and cognitive performance across taxa (Jerison, 1973; Deaner *et al.*, 2007). Endocranial size is measured as endocranial volume (ECV) or cranial capacity (measured in cc), where cranial capacity was traditionally measured using mustard seeds or the water displacement method (see Holloway *et al.*, 2004). Currently,

computer tomography (CT) and virtual reconstruction methods are used in combination to evaluate the ECV of most fragmentary fossil specimens (see Neubauer *et al.*, 2012).

Endocranial shape quantifies the spatial relationships (position, orientation and metric dimensions) between endocranial and exocortical morphology from an endocast. Traditionally, measurements included the cerebral length, maximum breadth/width, cerebral height and width of cerebellar lobes (Falk *et al.*, 2000). The endocranial vault is poor in anatomical reference points; which is further compromised by the lack of completeness of fossil samples. Several proposals have been made to solve this problem, the most promising of which employs virtual analytical methods to define surface features by geometric homology. In turn, this method enables additional observations on the shape of a region to be made. An example of such observation is the roundness or the lack of 'prominent protrusion' of the prefrontal lobe serving as an indication to researchers of the species being examined: this feature distinguishes human from non-human specimens (Holloway *et al.*, 2004; Specht *et al.*, 2007; Neubauer *et al.*, 2009; Zollikofer and Ponce de León, 2013; Bruner and Ogihara, 2018).

Imprints of cortical sulci and gyri provide information regarding brain organisation, and endocranial blood supply can be studied from the imprints of meningeal arteries and venous sinuses (see Holloway *et al.*, 2018; Beaudet *et al.*, 2019). Non-invasive imaging affords the possibility to quantify the spatial relationships between exocortical and endocranial morphology. Studying any of the abovementioned structures from endocasts do however pose problems: meningeal tissue, CSF, arteries and veins tend to blur direct imprints of the cerebral surface on the endocranial surface. The cortical sulci, which delineate the lobes and functional areas (e.g., the central sulcus and the lateral fissure) are often filled with blood vessels and CSF and therefore studying these in extant hominin endocasts has proven to be a difficult task (Holloway, 1978; Holloway *et al.*, 2004; Zollikofer and Ponce de León, 2013). Consequently, concerns have been addressed on the coincidental alignment of gyral and sulcal patterns with the bulges and furrows imprinted on the braincase (Le Gros Clark *et al.*, 1936).

2.4 Application of 3D imaging techniques to endocasts

Modern computer imaging methodologies have enabled significant progress in understanding human brain evolution (Neubauer, 2014). CT gained popularity in studying fossil remains from as early as the 1980's (see Conroy and Vannier, 1984) since it is advantageously minimally invasive, resulting in the original fossils not being harmed during the investigation process. It also allows for easy access to digital copies that can then be investigated by anyone at any time. CT scans of samples allow for easier preparation of the sample by electronically removing any sediment still present on the specimen that could not be removed during excavation. In the case of the cranial cavity being filled by sediment it can be segmented (digitally separated) from the bony elements to represent a natural endocast (Conroy and Vannier, 1984; Conroy *et al.*, 1990; Tobias, 2001; Weber and Bookstein, 2011; Zollikofer and Ponce de León, 2013; Neubauer, 2014). The increase in demand to study fossils in better detail eventually required higher resolution scans. Microfocus X-Ray tomography and synchrotron microtomography with resolutions as small as 0,7 μm (depending on type of sample, see Sanchez *et al.*, 2012) have gained popularity to study virtual endocasts with image resolutions of 100 μm or better (Fig. 2.6) (Neubauer, 2014). Virtual endocasts not only have the advantage of being non-invasive and easily distributable/accessible (see Falk *et al.*, 2005), since advanced algorithms also allow for convenient and easy analysis of shape by measuring distances between points on the virtual endocasts. This enables rapid calculation of volume, as well as correcting and adding missing fragments or even reconstructing the whole endocast using morphometrics (Weber and Bookstein, 2011; Zollikofer and Ponce de León, 2013; Neubauer, 2014; Holloway, 2018).

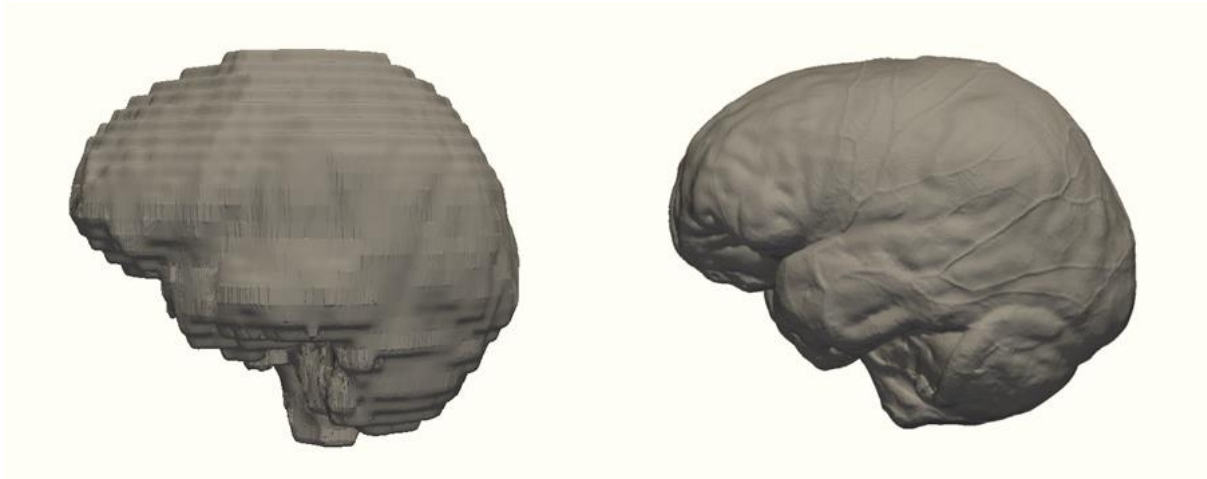


Figure 2.6: Extant human endocast generated from medical grade CT's (left) compared with an extant human endocast generated from micro CT's (right)

2.5 Multimodal brain atlases

Consistency of sulcal imprint interpretation on fossil endocasts remains a problem. Recent publications still dispute previously reported interpretations made on fossil endocasts after documenting sulci variation in chimpanzee brains (Falk *et al.*, 2018). Likewise, the immense intersubject variability in extant human brains has long been a challenge for neurosurgeons when trying to delineate cortical features during keyhole surgery (Ribas, 2010). To solve this problem, researchers have created population-specific brain atlases that provide a database where data from multiple subjects and modalities can be compared and analysed (Toga *et al.*, 2006).

Brain VISA (<http://brainvisa.info/web/index.html>) is an example of a user-friendly platform which enables researchers or clinicians to study brain data from multiple modalities (MRI, fMRI, EEG etc.) using various tools for processing and visualisation. It enables the investigators to share data with other laboratories and clinicians around the world (Cointepas, 2001; Rivière, 2009; Perrot *et al.*, 2011).

As described by Toga and Thomson (2001), three methods exist to form the foundation of population-based atlases. Firstly, **density-based approaches** focus on producing generalized representations of the anatomy by averaging the intensity of every voxel from multiple magnetic resonance images (MRI) and aligning the scans into a stereotaxic space to create an

average intensity MRI database. Unfortunately, high variability in the population results in blurring of individual cortical structures; causing negative implications in quantitative research. Secondly, **label-based approaches** (also known as statistical/probabilistic anatomy maps (SPAM)) involve large volumes of brain data (cortical structures) being manually segmented after the dataset is aligned in a stereotaxic space. By determining the proportion of subjects assigned a given anatomical label at each voxel position in the stereotaxic space, a probability map for the structures of interest can be created (Evans *et al.*, 1994). Finally, **deformation-based approaches** are based on a warping algorithm used to calculate a deformation map of a scan based on a reference scan optimised by the input atlas; matching cortical structures from one scan to their corresponding structure in another (reference) scan (Bookstein, 1989). This approach may shed light on the anatomical differences between population groups. In more complex cases, magnitude and directional biases of variations can be determined. Furthermore, assessments of the severity of structural variants outside the normal range can be made to determine if pathology is present (Bookstein, 1989; Evans *et al.*, 1994; Thompson and Toga, 1997; Thompson and Toga, 1999; Thompson *et al.*, 2000; Toga and Thompson, 2001).

Based on this knowledge, it would seem appropriate to adopt a statistical/probabilistic approach for this study, as it addresses the problem of intersubject variability and may therefore prove crucial in designing a probability map and potentially solve long-standing questions in palaeoneurology.

2.6 Aim:

The aim of this prospective study was to develop an extensive reference database of virtual endocranial cortical surface variations in extant humans and chimpanzees, based on intra-observer comparisons of visible sulci extracted from endocasts, in order to create a method for the automatic recognition of cortical imprints on fossil cranial endocasts.

2.7 Objectives:

The objectives of this study were:

1. To note and discuss sulcal patterns and the prevalence thereof on a South African formalin-fixed brain sample population.
2. To statistically compare cortical feature visibility between human brains and human brain endocasts.
3. To construct an atlas for extant human and chimpanzee endocasts, by including detailed percentages of cortical feature visibility on the endocasts.
4. To develop probability maps for illustrating and quantifying the intra-specific variation in humans and for every identifiable sulcus.
5. To design a reliable protocol for the automatic recognition of sulci in any given endocast based on the atlas created.

Chapter 3: Materials and Methods

3.1 Study Design

In this prospective study the sulci of formalin-fixed extant human brains from a South African sample population were documented in order to report on the relevant sulcal prevalence in a local sample set. This information, supplemented with that of other well-known brain atlases, were used for the primary goal of this study: to evaluate endocranial imprints on extant human and chimpanzee cranial endocasts by identifying cortical surface features using modern imaging techniques. A probability map of virtual endocranial cortical surface variation focusing on extant humans was developed, based on the results obtained, for the evaluation of fossil endocasts. The same method was evaluated on the common chimpanzee and bonobo crania.

3.2 Setting

Ethical clearance for this project was obtained from the Faculty of Health Sciences Research Ethics Committee, UP (certificate no. 339/2017) ([Appendix A](#)). This study was mainly conducted at the University of Pretoria (UP) where the Department of Anatomy's donated formalin-fixed human brain collection and the Pretoria bone collection and are housed. Brains (n = 61) were sampled and analysed from the human cadaver collection of the Department of Anatomy, UP. Through the AESOP+ (A European and South African Partnership on Heritage and Past+) project, we were able to collaborate with various European institutions and South African institutions. In a previous study, dry crania from the Pretoria Bone Collection were scanned at the Nuclear Energy Corporation of South Africa (Necsa), Pelindaba, in 2016 (see Beaudet *et al.*, 2016b). The chimpanzee scans were retrospectively collected from the Royal Museum of Central Africa, Tervuren, Belgium, in 2017 ([Appendix B](#)). The algorithm and software design were accomplished in collaboration with the Université Paul Sabatier (UPS), Toulouse, France. All endocasts (n = 58 + 22) were extracted and analysed using modern imaging software algorithms at the Necsa facility and partially at Centre de Recherche Cerveau & Cognition (CerCo; UMR5549) (UPS) and the Toulouse Mathematics Institute (UPS).

3.3 Sample Population

Formalin-fixed human brains (n = 61) harvested during the undergraduate dissection course during the duration of this study at the Department of Anatomy, UP, consisting of 27 females and 33 males, were analysed. Endocasts of 58 adult human crania from the Pretoria Bone Collection consisting of 20 females and 38 male specimens of European and African ancestry within an age range of 30 to 94 years were selected from a dataset that had been previously extracted and reconstructed for a related study (Beaudet *et al.*, 2016b). Of twenty-two (11 males and 11 females, respectively) wild-shot African *Pan* (chimpanzee) specimens from the mammal bone collection at the Royal Museum for Central Africa (Tervuren, Belgium) that were previously collected by the museum and subsequently scanned, 22 endocasts developed therefrom were processed for this study. This sample consisted of taxa *Pan paniscus*, *Pan troglodytes verus*, *Pan troglodytes troglodytes* and *Pan troglodytes schweinfurthii*. A summary of all samples that were collected for this study is available in Table 3.1.

Table 3.1: Summary of all samples collected

Population Group	Number of specimens in sample population
<i>Homo sapiens</i>	58 endocasts and 61 brains
<i>Pan paniscus</i>	10 endocasts
<i>Pan troglodytes verus</i>	2 endocasts
<i>Pan troglodytes troglodytes</i>	5 endocasts
<i>Pan troglodytes schweinfurthii</i>	5 endocasts
Total	140 samples

3.4 Exclusion criteria

Formalin-fixed brains were excluded where previous known pathology was expected to affect sulcal visibility (e.g. meningioma) and where the preservation quality of the brain after it had been extracted from the donor bodies (e.g. damage to a cortical lobe of interest).

Endocasts were excluded based on observed presence of any distortions on the endocasts due to deformations of the cranial vault that had resulted from any antemortem or post-mortem pathology (e.g. Paget disease – see Paget, 1877), especially hyperostosis frontalis interna (see Hershkovitz *et al.*, 1999) which was positively identified in some of the dry crania. Other exclusions were made based on visual inspection; such as the level of clarity of surface feature impressions on the endocast or the prominence of the middle meningeal artery impression on the endocasts.

3.5 Equipment/Software

A digital camera was used to photographically document all the relevant surfaces of the formalin-fixed brains after they were extracted, after the arachnoid mater was cleaned from the brain surface using a standard dissection kit. To analyse the photos an open source image processing software *ImageJ* (<https://imagej.nih.gov/ij/>) was used.

The Nikon XTH 225 ST micro-focus X-ray computer tomography facility (MIXRAD) housed at Necsa (see Hoffman and de Beer, 2012) was used to scan the intact dry crania of extant humans. Micro-CT was chosen due to its ability to obtain information at a high resolution (see section [2.4](#)). Software such as Nikon's *CT-Pro* was used to reconstruct the raw 2D projection images into a 3D volume file. Dry common chimpanzee and bonobo crania were scanned by **micro-focus X-ray computer tomography** facility at the Centre for X-ray Tomography of the Ghent University (UGCT). *Aviso v9.0* (FEI Visualization Sciences Group Inc.), a 3D visualisation and analysis software, was used to change the format of the imaging files for easier handling and importation into other software for analysis. *Endex*, an automatic segmentation software developed by Gilles Gesquière and Gérard Subsol (<https://perso.liris.cnrs.fr/gilles.gesquiere/>

wiki/doku.php?id=endex), was used to digitally extract the virtual endocast from the cranial cavity of extant humans (Subsol *et al.*, 2010; Beaudet *et al.*, 2016a). A similar protocol was used in this study for extraction of the common chimpanzee and bonobo endocasts. Yoshizawa's algorithm for automatic detection of crest and base lines was used to detect any surface features present on the endocasts (Yoshizawa *et al.*, 2008) (<http://www.riken.jp/briect/Yoshizawa/Research/Crest.html>). A custom script in **Matlab R2013a** (Mathworks) was used to remove any non-biological structures that were detected by the algorithm on the endocast (Fig. 3.1; <https://gitlab.com/jeandumoncel/curve-editor>). **ParaView** (<http://www.paraview.org/>) is an open source easy to use software that was used to visualise the endocasts.

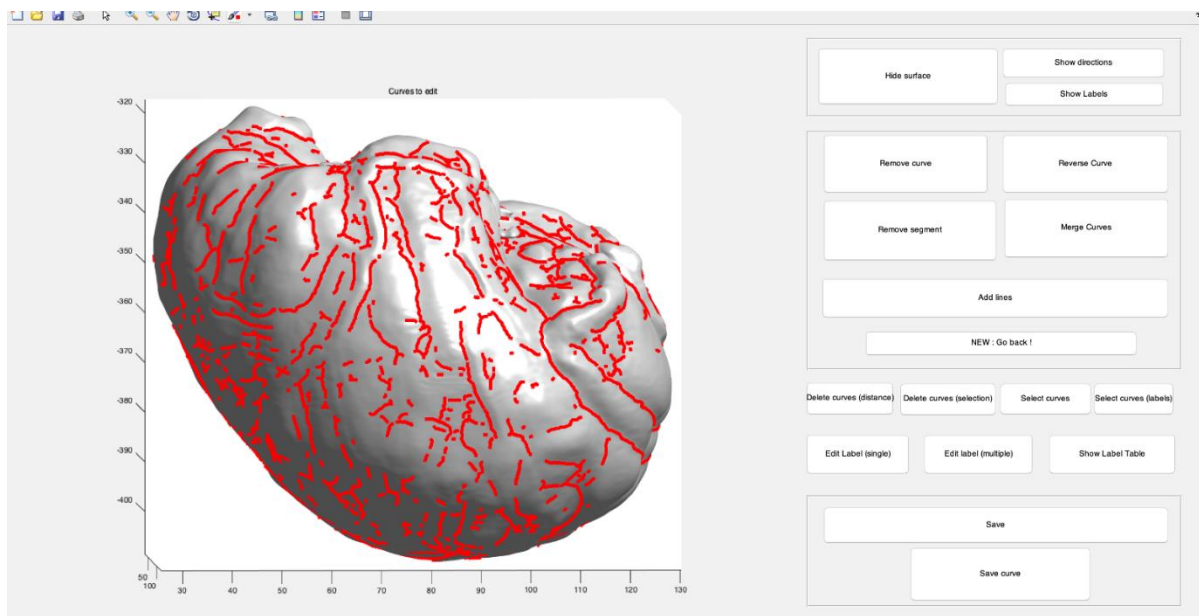


Figure 3.1: Screenshot of the custom script used in Matlab to label curves representing sulci and delete unwanted artefacts (Beaudet *et al.*, 2016a)

3.6 Procedure

3.6.1 Formalin-fixed brains:

Brains were extracted using a standard dissection method (Tank, 2012) to ensure maintenance of integrity during the various dissection courses that ran through the year in the Department of Anatomy, UP. The meninges and lenticulostriate vessels were removed to expose the surface of the underlying cortex. Images of the superolateral surface and the orbital part of the basal surface of the cortex were captured at various overlapping angles using a digital camera. These images were then analysed using Image J to manually identify the presence of cortical sulci and gyri (refer to section [3.5](#)).

3.6.2 Endocasts:

Dry human and *Pan* crania have been scanned using micro-CT at a spatial resolution ranging from 94 to 123 μm^3 and 65 to 85 μm^3 respectively. This imaging technique produces high quality 2D X-ray images in TIFF format (Fig. 3.2). After scanning the skulls, the TIFF stack was imported into CT-Pro where the image stack was converted into a 3D volume file that could be imported into any CT visualisation and analysis software. Aviso v9.0 (FEI Visualization Sciences Group Inc.) was used to convert the 3D volume file of the crania into an object file (.obj) for easier manipulation. This object file was imported to Endex, which was used to extract the endocast from the cranium automatically (Fig. 3.2 and 3.3A) (Subsol *et al.*, 2010). Endex performs this automated extraction by placing a surface mesh composed of 3D vertices into the middle of the scanned data of interest, represented by a set of 3D points. The surface mesh then expands through attraction of the mesh's vertices towards the scanned data in combination with an internal force that pushes the mesh out towards the data, which ensures maximal refinement of the endocast surface. More vertices are added in succession in the expanded mesh once the distance between existing vertices has extended too far, to ensure capturing of more intricate details on the endocast (Fig. 3.3B).

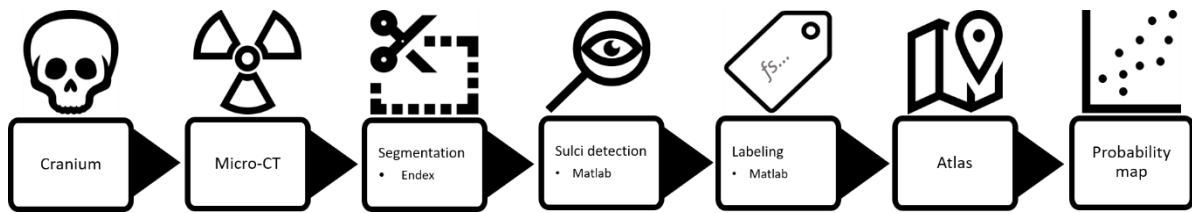


Figure 3.2: Summary of procedure followed for endocasts

After the endocasts were extracted, a semi-automatic detection method was used to study the sulcal imprints based on previous studies. The algorithm automatically detects topographical variations, for example, crest lines on meshes for indication of cortical relief in endocasts (Fig. 3.2C and 3.3) (Yoshizawa *et al.*, 2007; Yoshizawa *et al.*, 2008). A custom script was used in Matlab R2013a (Mathworks) to manually identify relevant surface features as well as remove any unwanted artefacts (e.g., meningeal arteries) using an application that was made available to us by AMIS (Anthropobiologie Moléculaire et d'Imagerie de Synthèse – UMR5288), UPS, France (Fig. 3.2 and 3.3D; Beaudet *et al.*, 2016a). ParaView (less resource-demanding visualisation software) was used to visualise which cortical sulci were identified in the endocasts.

Finally, a protocol was developed for computing probability maps based on the atlases and ongoing collaboration with the research team *Images et modèles pour l'exploration du cerveau* (IMPEC), based at CerCo, UPS and Toulouse Mathematics Institute (UPS). To calculate the anatomical variability of sulcal imprints on endocasts, the average shape of the entire sample of endocasts had to be calculated which was considered as the common template on which the curves (representing the sulcal imprint) was projected. Finally, the spatial variability of each labelled sulcal imprint was quantified (Fig. 3.2).

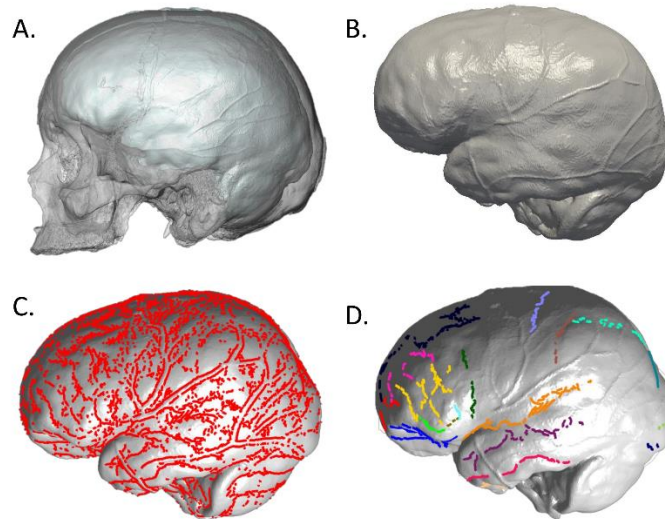


Figure 3.3: Automatic extraction of an extant human endocast using Endex (A). Resulting endocast mesh (B). Application of crest line detection algorithm (C). Endocast after cleaning of crest lines and labelling (D) (de Jager *et al.*, 2019)

3.6.2.1 Average endocast surface estimation

All the meshes representing the endocasts, and curve sets representing the sulcal imprints (both in .vtk format) were rigidly aligned and scaled during the extraction and detection process. Due to the anatomical variability of each endocast, the average shape of the whole endocast sample set had to be calculated. To achieve this, for each mesh, a void 200 x 200 x 200 voxels 3D image (volume file) was generated. The correspondence between the mesh's (.vtk format) coordinates and the 3D image coordinates was defined so that all meshes were represented as 3D images with a margin of about 10 voxels ($\pm 1\text{mm}$). A value of 1 was assigned to the voxels in the image which corresponded to each node on the corresponding mesh which ensured the meshes were densely sampled in the 3D images. The resulting 3D images were then smoothed using a Gaussian filter with a standard deviation of 5 voxels ($\pm 0.5\text{mm}$).

Once all the 3D images were computed, the average shape was defined as the barycentre of these images in a specific Riemannian-shaped space following the method of Fiot *et al.*, 2014 and Vialard *et al.*, 2012b. A 3D image was randomly picked out of the sample set to be the initial guess average image. It was then iteratively deformed towards the Karcher mean (Karcher 1977) of all the images of the entire sample. The main advantage of this method was that it fully preserved the topology of the cranial structures.

In practice, this iterative method was performed as follows: We denote E_{cur} as the average image at the current iteration and I_i , the n other brain images $I(M_i)$. We initiated E_{cur} as equal to E_{init} . Diffeomorphic registration of E_{cur} on the different images I_n was then performed using the method of Vialard *et al.* (2012a), which resulted in n scalar fields encoding the deformation and denoted initial momenta m_i . At each iteration, the current average E_{cur} is then updated by being deformed using the information in the average momentum $m_{cur} = \text{mean}(m_1, \dots, m_n)$. This process is repeated until E_{cur} does not present any significant deformation. As shown in (Vialard *et al.*, 2012a), this process typically converges after about 5 to 10 iterations for skulls. The average shape E_{av} is finally equal to E_{cur} at convergence.

3.6.2.2 Sulcal imprint variability estimation

Once average shape was computed, we denoted ϕ the displacement field (deformation) between M_i and E_{av} which was computed using any standard registration algorithm. In this study we used a classic Demons approach (Thirion, 1998).

Each curve set C_i was projected in the common template domain using ϕ . This projected set was denoted as $P(C_i)$. Considering a specific sulcal label (L) out of all labels contained in the entire set of labels L_i-j . Using a similar process followed to project the meshes M_i in the images $I(M_i)$, we projected all the sulci coordinates with label (L) in an image $I(L)$. The resulting image was smoothed with a Gaussian filter with the standard deviation of 5 voxels and the intensities were linearly resampled between 0 and 100. Each image subsequently represented the spatial variability of each observed sulcus.

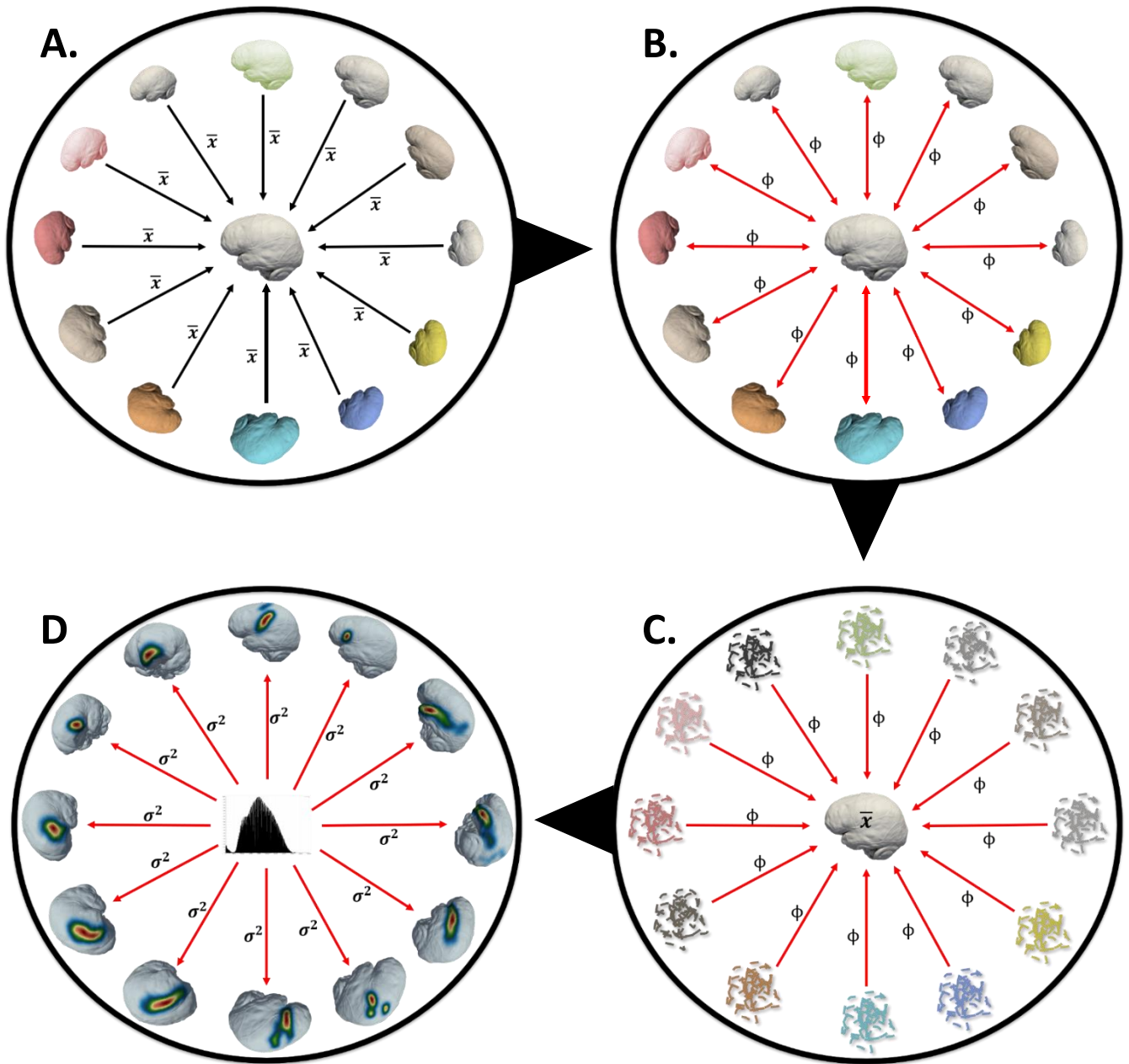


Figure 3.4: Summary of process followed in 3.6.2.1 and 3.6.2.2. A: The average surface was calculated by deforming all the endocasts towards the Karcher mean (\bar{x}) of all images in sample; B: Calculate the deformation (where ϕ represents an endocast-specific value) value for each endocast. C: Project all curves (sulci) to common template using ϕ ; D: Variance (σ^2) of each imprint on the endocast can be calculated

3.7 Observations

On the formalin-fixed human brain samples, all sulcal and gyral convolutions were taken note of through visual inspection, using the same criteria as for the endocasts, attention was paid to variations in the convolutions. For the endocasts, observations were made to identify primary, secondary and tertiary sulcal impressions (referred to as ridges and ravines) present on the external surface of the endocast based on works by (Connolly, 1950, Ono *et al.*, 1990). An example of generic observations that were made can be seen below:

- indication of presence (or absence) of each sulcus (left and right),
- noting the number of segments observed (left and right),
- landmarking of *anterior* connections in the two human groups' (brain and endocast) sample population as well as the *Pan* endocast population according to known convolutions with reference to published literature, and comparing the prevalence of these observations with other studies,
- landmarking of *posterior* connections in the two human groups' (brain and endocast) sample population as well as the *Pan* endocast population according to known convolutions with reference to published literature, and comparing the prevalence of these observations with other studies,
- presence (or absence), frequency and direction of side branch connections within the sulcus.

3.8 Statistical analysis

The planned sample size was 60 formalin-fixed brains and 58 endocasts. For estimating the reliability of identifying cortical features on the endocasts, a sample of 60 scans, with an expected agreement (Ono *et al.*, 1990) of at least 90% with previous brain atlases (e.g. Ono *et al.*, 1990), will result in a precision of +/- 8% for the sensitivity estimate.

Additionally, basic descriptive statistics such as the mean was used to describe the average prevalence of a specific sulcus. Mode was used to describe the most common sulcal traits observed. The minimum and maximum frequencies were used to describe the minimum and maximum occurrences of a certain sulcal trait.

An open source calculator (<http://www.quantpsy.org/chisq/chisq.htm>) was used to perform the Chi-Square test (Preacher, 2001) in order to test if there is a significant difference between the frequency of sulci observed on the left cerebral hemisphere compared to the right and if there is a significant difference between the frequency of sulci observed in male samples vs. female samples in both the brain sample population, extant human endocast population and *Pan* endocast population. Since we expected no statistically significant variation of observable sulcal morphology between left and right hemispheres, nor between female and male brain specimens, this null hypothesis was rejected where variations observed exceeded a p-value of 0.05 ($p < 0.05$). In cases where the at least 20% of the expected frequencies are less than 5 we incorporated the Yates's correction for continuity. For the probability maps refer to sections [3.6.2.1](#) and [3.6.2.2](#).

Chapter 4: Results

The results to following are presented in the same order as the objectives for this study.

4.1 Extant human brain

Data from 60 formalin-fixed brains were collected over a two-year period. We excluded 17 brains due to exclusion criteria (refer to section [3.4](#)) and limitations. By studying the sulcal patterns 43 brains (18 females, 25 males) with an age range of 46 to 95 years ([Appendix C](#)) we observed no significant difference in the presence of a sulcus between male and female brains as well as left and right hemispheres ($p < 0,05$). A summary of our observations on formalin-fixed brain population can be seen in Table 4.1 – 4.6.

Table 4.1: Summary of sulci observed on each hemisphere of the frontal lobe

Frontal lobe		
Orbital Sulcus	<ul style="list-style-type: none"> • Presence of transverse sulcus = 92% • Posterior directed sulci: <ul style="list-style-type: none"> ○ Max. sulci: Left = 4 Right = 3 ○ Mode = 2 sulci ○ Presence of free sulcus = 27% • Anterior directed sulci: <ul style="list-style-type: none"> ○ Max. sulci: Left = 4 Right = 3 ○ Mode = 2 sulci ○ Division of medial sulcus = 34% ○ Division of lateral sulcus = 22% ○ Common no. of free sulci = 1 	Appendix F1
Fronto-orbital sulcus (sensu Ono <i>et al.</i>, 1990)	<ul style="list-style-type: none"> • Incidence = 73% • Left = 70% Right = 77% • Connections: <ul style="list-style-type: none"> ○ Inferior frontal sulcus = 24% ○ Fronto-marginal = 9% ○ Middle frontal = 8% 	Appendix F2
Fronto-marginal sulcus	<ul style="list-style-type: none"> • Incidence = 94% • Left = 93% Right = 95% • Connections: <ul style="list-style-type: none"> ○ Middle frontal = 62% ○ Orbital = 13% 	Appendix F2

Superior frontal sulcus	<ul style="list-style-type: none"> • Incidence = 97% • Left = 98% Right = 95% • Max. no. of segments = 4 • Continuity = 41% • Connections: <ul style="list-style-type: none"> ○ Precentral = 89% ○ Middle frontal = 45% 	Appendix F3
Inferior frontal sulcus	<ul style="list-style-type: none"> • Incidence = 100% • Max. no. of segments = 3 segments • Continuity = 50% • Connections: <ul style="list-style-type: none"> ○ Inferior postcentral = 78% ○ Middle frontal = 44% ○ Diagonal = 23% 	Appendix F3
Middle frontal sulcus	<ul style="list-style-type: none"> • Incidence = 100% • Interrupted = 65% • Connections: <ul style="list-style-type: none"> ○ Fronto-marginal = 80% ○ Precentral = 56% ○ Inferior frontal = 54% ○ Superior frontal = 51% 	Appendix F3
Precentral sulcus	<ul style="list-style-type: none"> • Incidence = 100% • Continuity = 25% • Segments: <ul style="list-style-type: none"> ○ Superior precentral = 83% ○ Inferior precentral = 87% ○ Middle precentral = 19% ○ Marginal precentral = 15% ○ Medial precentral = 43% • Connections: <ul style="list-style-type: none"> ○ Central = 23% ○ Diagonal = 16% ○ Sylvian = 5% 	Appendix F4
Diagonal sulcus	<ul style="list-style-type: none"> • Incidence = 72% • Left = 74% Right = 70% 	Appendix F3 and F6

Table 4.2: Summary observations for the Sylvian fissure on each hemisphere

Sylvian fissure	<ul style="list-style-type: none"> • Incidence = 100% • Branches: <ul style="list-style-type: none"> ○ Horizontal ramus = 97% (L = 100%; R = 93%) ○ Ascending ramus = 97% (L = 100%; R = 93%) ○ Anterior subcentral = 56% ○ Posterior subcentral = 54% ○ Transverse temporal = 61% ○ Posterior ascending ramus = 76% • Connections: <ul style="list-style-type: none"> ○ Postcentral = 47% ○ Precentral = 26% ○ Central = 6% 	Appendix F6
------------------------	--	-----------------------------

Table 4.3: Summary observations for the central sulcus on each hemisphere

Central sulcus	<ul style="list-style-type: none"> • Incidence = 100% • Continuity = 97% • Continuous with Sylvian fissure = 7% • Sup. extension to medial surface = 67% • Max. no. of side branches = 6 • Connections: <ul style="list-style-type: none"> ○ Precentral = 41% ○ Postcentral = 7% ○ Superior frontal = 6% 	Appendix F4
-----------------------	--	-----------------------------

Table 4.4: Summarising sulci observed on each hemisphere of the parietal lobe

Parietal lobe		
Postcentral sulcus	<ul style="list-style-type: none"> • Incidence = 100% • Continuity = 33% • Max. no. of segments = 3 • Connections: <ul style="list-style-type: none"> ○ Intraparietal = 92% ○ Sylvian = 35% ○ Central = 17% 	Appendix F4
Intraparietal sulcus	<ul style="list-style-type: none"> • Incidence = 100% • Continuity = 57% • Max. segments = 2 • Max. side branches: <ul style="list-style-type: none"> ○ Superior = 6 ○ Inferior = 4 • Connections: <ul style="list-style-type: none"> ○ Postcentral = 80% ○ Transverse occipital = 91% ○ Sup. temporal = 21% 	Appendix F4

Table 4.5: Summary sulci observed on each hemisphere on the occipital lobe

Occipital lobe		
Transverse occipital sulcus	<ul style="list-style-type: none"> • Incidence = 100% • Contribution to Lunate = 37% 	Appendix G
Lateral/Inferior occipital sulcus	<ul style="list-style-type: none"> • Incidence = 100% • Max. sulci observed = 3 sulci • Contribution to Lunate = 21% 	Appendix G
Lunate sulcus	<ul style="list-style-type: none"> • Incidence = 71% • Left = 65% Right = 77% • Possibly true = 9% 	Appendix F7 and Appendix G
Lateral calcarine sulcus	<ul style="list-style-type: none"> • Incidence = 83% • Left = 77% Right = 88% 	Appendix G
Retro-calcarine sulcus	<ul style="list-style-type: none"> • Incidence = 56% • Left = 60% Right = 51% 	Appendix G

Table 4.6: Summarising sulci observed on each hemisphere on the temporal lobe

Temporal lobe		
Superior temporal sulcus	<ul style="list-style-type: none"> • Incidence = 100% • Continuity = 48% • Max. no. segments = 4 (Mode = 1) • Free superior sulcus = 41% • Max. number of posterior rami = 3 (Mode = 3) • Connections: <ul style="list-style-type: none"> ○ Inferior temporal = 79% ○ Intraparietal = 28% ○ Sylvian fissure = 13% 	Appendix F5
Inferior temporal sulcus	<ul style="list-style-type: none"> • Incidence = 100% • Max. no. segments = 7 (Mode = 3) • Continuous with occipital sulci = 40% 	Appendix F5

4.2 Extant human endocasts

The following results are published in the Journal of Anatomy (de Jager *et al.*, 2019; [Appendix H](#)) of which the preliminary results were presented in the form of a poster (de Jager *et al.*, 2018; [Appendix I](#)). Out of the 58 endocasts available, only 20 endocasts were analysed (10 females, 10 males) after exclusions were made based on the exclusion criteria described in section [3.4](#), and after re-evaluation of project time constraints. These 20 endocasts consisted of human specimens that spanned an age range of 30 to 80 years ([Appendix D](#)). The frequencies of sulci identified on the left (LH) and right (RH) hemispheres of the crania are alphabetically listed in Table 4.7 below.

Table 4.7: Frequency of sulci observed for left and right hemispheres in humans (de Jager *et al.*, 2019)

Sulcus	Left	Right
anterior horizontal ramus (<i>hr</i>)	40%	20%
ascending ramus (<i>ar</i>)	40%	20%
central (<i>c</i>)	55%	50%
collateral (<i>col</i>)	25%	0%
fronto-marginal (<i>W</i>)	85%	100%
fronto-orbital (<i>fo</i>)	75%	60%
inferior frontal (<i>if</i>)	85%	90%
inferior temporal (<i>it</i>)	100%	95%
middle frontal (<i>fm</i>)	90%	75%
intraparietal (<i>ip</i>)	30%	15%
lateral calcarine (<i>lc</i>)	55%	20%
Lateral/inferior occipital (<i>oci</i>)	50%	60%
lunate (<i>L</i>)	80%	70%
occipitotemporal (<i>oct</i>)	35%	45%
orbital sulci (<i>o</i>)	100%	100%
postcentral (<i>pt</i>)	20%	15%
precentral (<i>pc</i>)	35%	40%
retro-calcarine (<i>rc</i>)	20%	10%
rhinal (<i>rh</i>)	25%	60%
superior frontal (<i>sf</i>)	95%	90%
superior temporal (<i>st</i>)	75%	90%
Sylvian fissure (<i>S</i>)	95%	85%
transverse occipital (<i>otc</i>)	70%	55%

4.2.1 Frontal lobes

The of the branches of the orbital sulcus (*o*) impressions was identified on the orbital surface of all cranial endocasts, a clear transverse orbital sulcus impression was identified on nine crania, resulting in the generally known “H” or “Y” pattern. The olfactory sulcus was not considered in any of the crania due to the distortion caused by the impression from the cribriform plate.

The fronto-orbital sulcus of the frontal lobe (*sensu* Ono *et al.*, 1990) was clearly identified in 75% of LHs and 60% of RHs (Fig. 4.1 – 4.2). The fronto-marginal sulcus was identified in 85% of LHs and in 100% of RHs (Fig. 4.1h).

The superior frontal sulcus was clearly identified in 95% of LHs and in 90% of RHs. In addition, connections between the superior frontal sulcus and the fronto-marginal sulcus (n=12), middle frontal sulcus (n=7) and the precentral sulcus (n=2) were observed (Fig. 4.1 – 4.2).

The middle frontal sulcus was identified in 90% of LHs and in 75% of RHs, where segmental patterns (n=13) were most frequently observed (Fig. 4.2a).

Impressions of the inferior frontal sulcus were identified in 85% of LHs and in 90% of RHs and up to seven side branches were observed in one cranium; some of which extended onto the orbital surface and others connecting with the middle frontal sulcus (Fig. 4.2r). The inferior frontal sulcus was not clearly defined in five crania; which may be due to distortion caused by overlaying blood vessels (Fig. 4.2f). The precentral sulcus was observed in only 35% of the LHs and 40% of the RHs (Fig. 4.1 – 4.2).

The Sylvian fissure was clearly identified in 95% of LHs and 85% of RHs. The anterior horizontal ramus and ascending ramus was identified in only eight LHs and four RHs (Fig. 4.1 – 4.2).

4.2.2 Parietal lobes

The central sulcus was identified in 55% of LHs and 50% of the RHs (Fig. 4.1). The postcentral sulcus was observed in 20% of LHs and 15% of RHs (Fig. 4.1a). The intraparietal sulcus was identified on the LH of six crania and on the RH of three crania (Fig. 4.1a). Identification of the transverse occipital sulcus, or posterior branch of the intraparietal sulcus was possible in 70% of LHs and 55% of RHs (Fig. 4.1e-f).

4.2.3 Occipital lobes

The lateral/inferior occipital sulcus was identified in 50% of LHs and 60% of RHs, as a small sulcus along the most lateral and inferior border of the occipital lobe. Fragments of the lunate sulcus was identified in 80% of LHs and 70% of RHs (Fig. 4.1 – 4.2). Medial to the lunate sulcus, the lateral calcarine sulcus (LHs= 55%; RHs= 20%) and retro-calcarine sulcus (LHs= 20%; RHs= 10%) was identified.

4.2.4 Temporal lobes

The superior temporal sulcus was observed in 75% of LHs and 90% of RHs, with the anterior segment clearly imprinted. Similarly, the inferior temporal sulcus was observed in 100% of LHs and 95% of RHs with most crania exhibiting an anterior extension to the temporal pole (Fig. 4.1 – 4.2). When observing the basal surface of the temporal lobe, the rhinal sulcus was identified in 25% of LHs and 60% of RHs. The rhinal sulcus is frequently subject to a substantial degree of distortion due to the presence of the middle meningeal artery. Similar results were observed for the collateral sulcus (LHs= 25%; RHs= 0%) and the occipitotemporal sulcus (LHs= 35%; RHs= 45%).

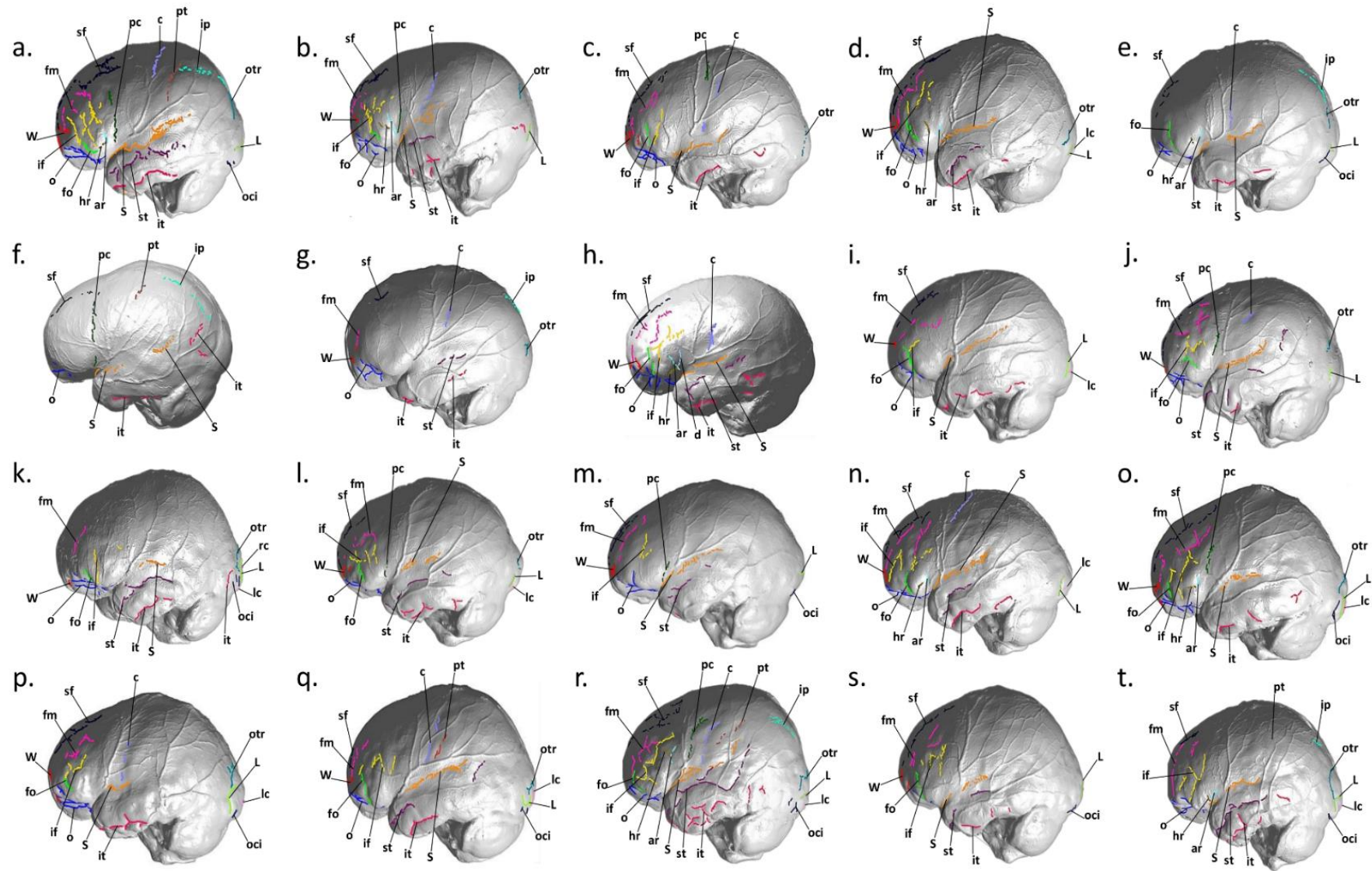


Figure 4.1: Sulcal imprints observed on the left hemisphere of twenty individuals. ar=ascending ramus, c=central, d=diagonal, W=fronto-marginal, fo=fronto-orbital, hr=anterior horizontal ramus, if=inferior frontal, ip=intraparietal, it=inferior temporal, L=Lunate, lc=lateral calcarine, fm=middle frontal, o=orbital, oci= lateral/inferior occipital, otr=transverse occipital, pc=precentral, pt=postcentral, rc=retro-calcarine, S=Sylvian fissure, sf=superior frontal, st=superior temporal (de Jager et al., 2019) 58

4.2.5 Left vs. Right hemisphere

Left-right hemisphere asymmetry was noted for the lateral calcarine sulcus (LHs= 55%; RHs= 20%, $p<0.05$), the rhinal sulcus (LHs= 25%; RHs= 60%, $p<0.05$) and the collateral sulcus (LHs= 20%; RHs= 0% $p<0.05$) (Fig. 4.3).

4.2.6 Male vs. Female

No significant differences in sulcal patterns were observed between male and female crania ($p>0.05$). In general, sulci were more readily identified in female (~3% more frequent) crania compared to male crania (Fig. 4.4). Sex specific differences were noted in the RHs in the impression of the fronto-orbital sulcus (M= 40%; F= 80%), precentral sulcus (M= 50%; F= 30%), transverse occipital sulcus (M= 40%; F= 70%), lunate sulcus (M= 80%; F= 60%), lateral calcarine (M= 30%; F= 10%), superior temporal sulcus (M= 80%; F= 100%), rhinal sulcus (M= 50%; F= 70%), occipitotemporal sulcus (M= 30%; F= 60%) and ascending ramus (M= 30%; F= 10%). Sex specific differences were noted in the LHs in the impression of the precentral sulcus (M= 20%; F= 50%), postcentral sulcus (M= 30%; F= 10%), intraparietal sulcus (M= 40%; F= 20%), transverse occipital (M= 60%; F= 80%), lunate sulcus (M= 70%; F= 90%), retro-calcarine sulcus (M= 30%; F= 10%), anterior horizontal ramus (M= 30%; F= 50%) and ascending ramus (M= 30%; F= 50%).

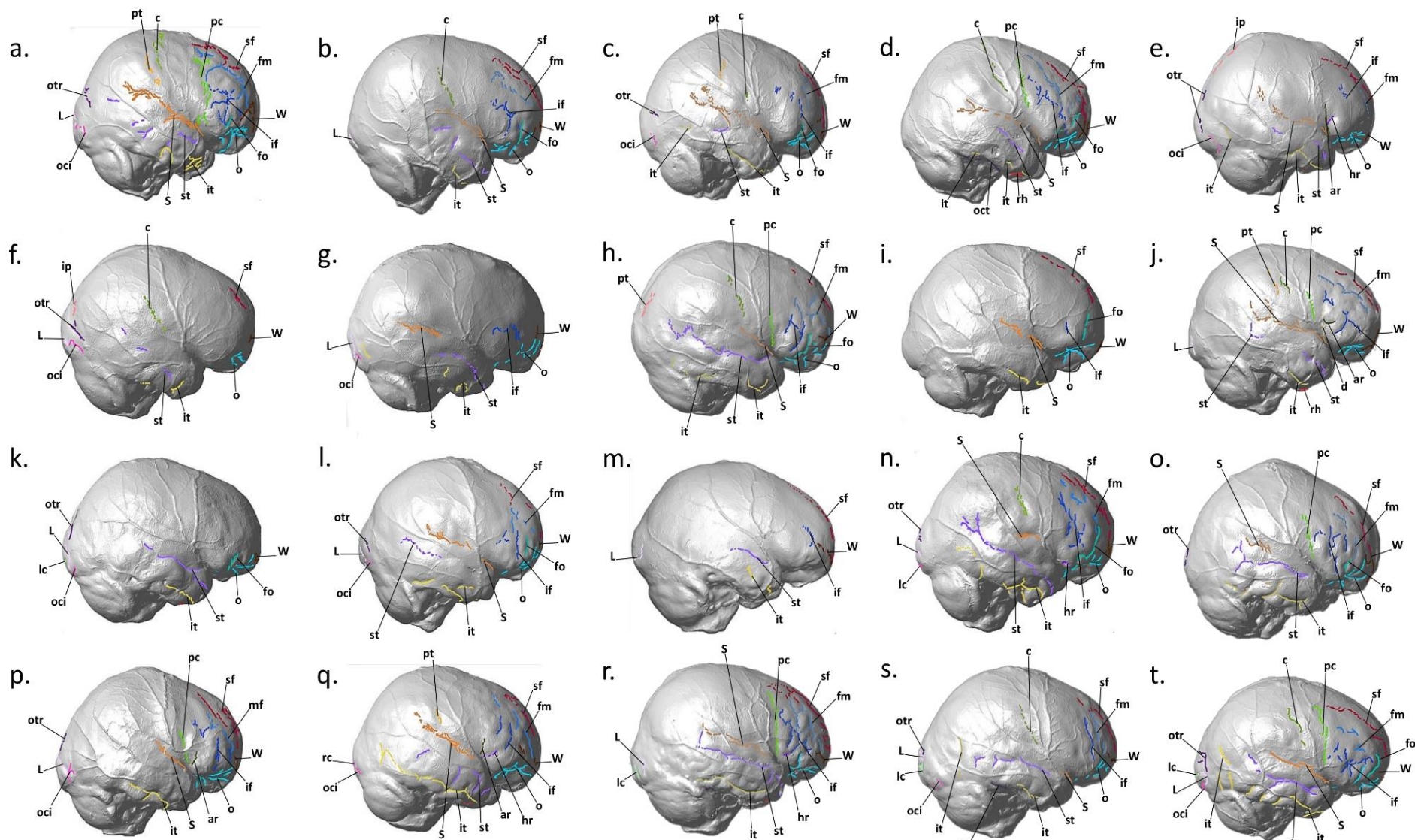


Figure 4.2: Sulcal imprints observed on the right hemisphere of twenty individuals. ar=ascending ramus, c=central, d=diagonal, W=fronto-marginal, fo=fronto-orbital, hr=anterior horizontal ramus, if=inferior frontal, ip=intraparietal, it=inferior temporal, L=Lunate, lc=lateral calcarine, fm=middle frontal, o=orbital, oci=lateral/inferior occipital, oct=occipitotemporal, otr=transverse occipital, pc=precentral, pt=postcentral, rc=retro-calcarine, rh=rhinal, S=Sylvian fissure, sf=superior frontal, st=superior temporal (de Jager et al., 2019)

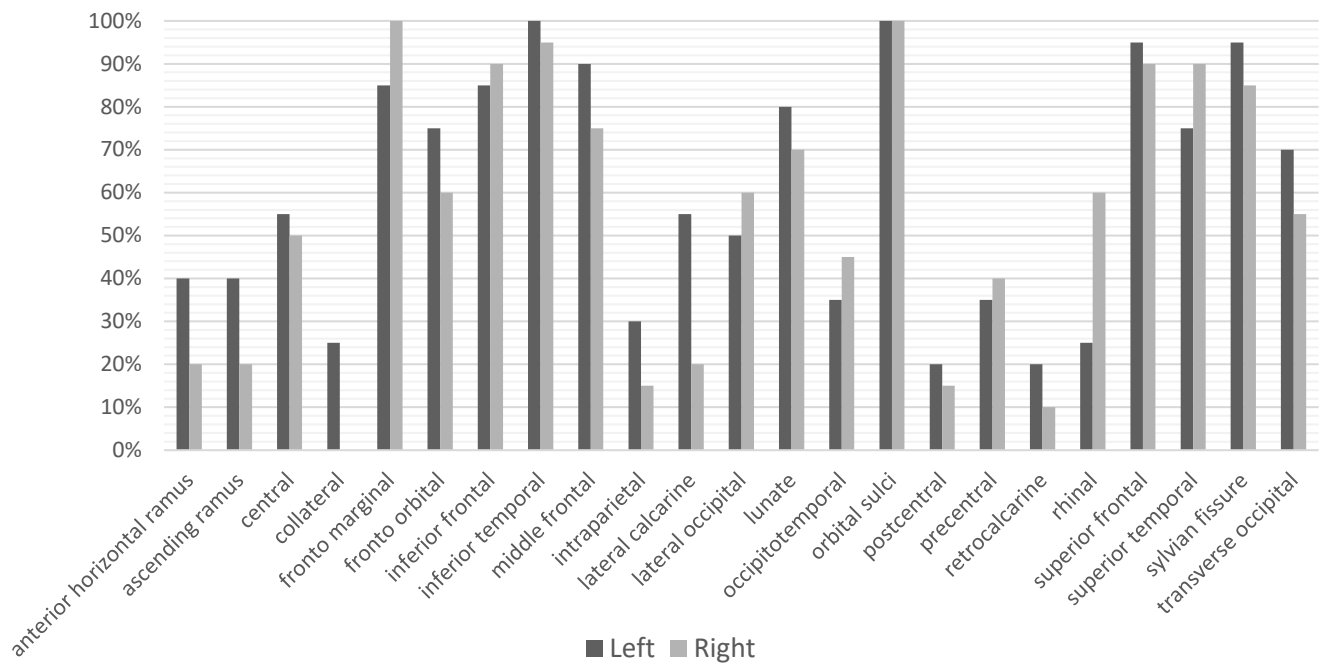


Figure 4.3: Frequency of sulci observed in the left and right hemispheres of human endocasts (de Jager et al., 2019)

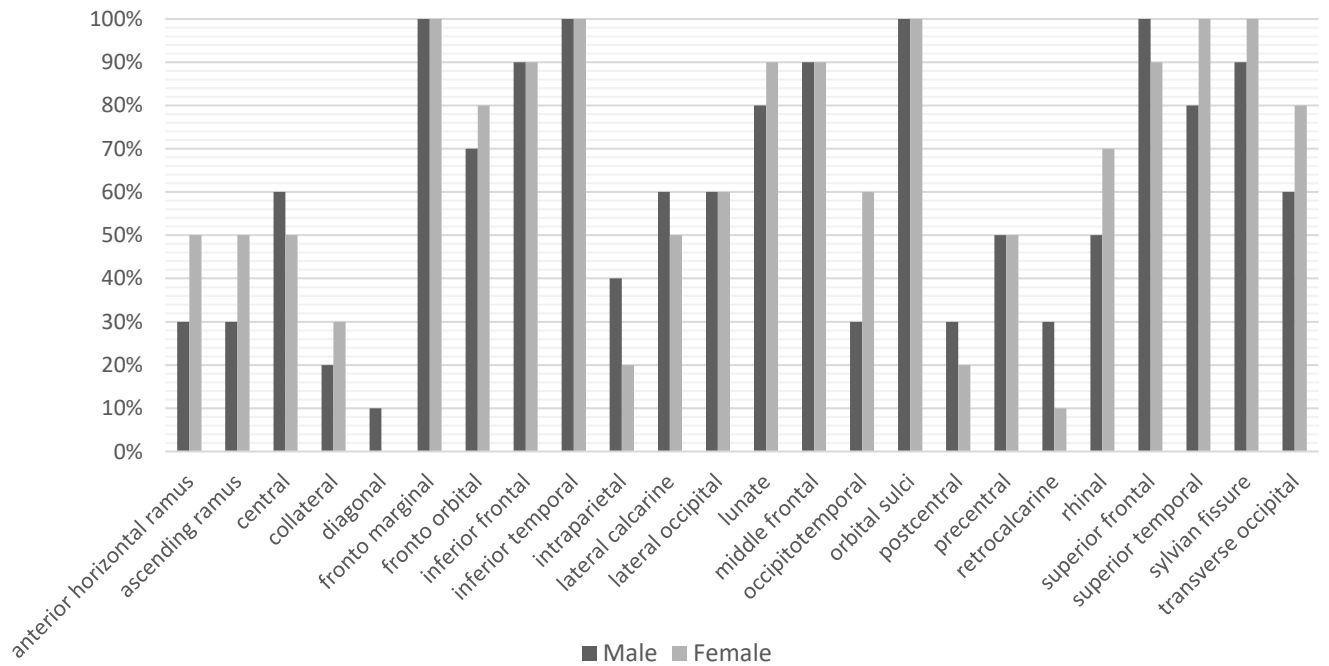


Figure 4.4: Frequency of sulci observed in male and female human endocasts (de Jager et al., 2019)

4.3 *Pan* (Chimpanzee/Bonobo)

Endocasts were extracted from 22 scanned crania, 16 endocasts were excluded based on distortion due to damaged cranial cavities ([Appendix E](#)). For the purpose of this study we documented the sulcal imprint variation on six *Pan* endocasts. For all the sulci the null hypothesis could not be rejected and therefore no significant difference can be seen in the occurrence of sulcal impressions between left and right hemispheres (Fig. 4.5) Due to sample constraints we did not test for significant differences between male and female endocasts.

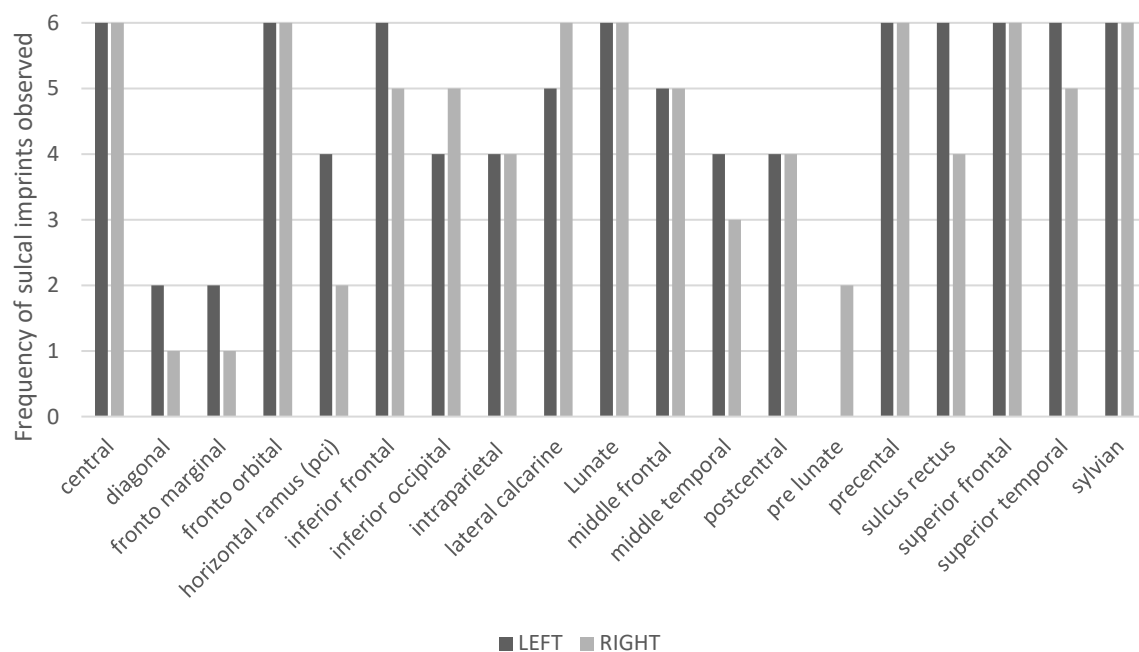


Figure 4.5: Frequency of sulcal imprints observed on six chimpanzee endocasts

4.3.1 Frontal lobe

Imprints of major sulci of the frontal lobe such as precentral sulcus, superior-, middle- and inferior frontal sulcus as well as the sulcus rectus were clearly identified on all the endocasts (Fig. 4.5). The fronto-orbital sulcus could be identified on all six endocasts and the horizontal ramus of precentral sulcus was identified in more than half of the endocasts on the LH and only in two on the RH. Imprints of the fronto-marginal sulcus and the diagonal sulcus could be identified only two of the endocasts endocasts.

The Sylvian fissure could be identified in all six endocasts. In most cases a segmental imprint could be identified, obliquely dividing the temporal lobe from the rest of the hemisphere (Fig. 4.6E).

4.3.2 Parietal lobe:

The central sulcus could be identified on all the endocasts, in two endocasts a more vertical imprint can be clearly seen marking the border between the frontal- and parietal lobes (Fig. 5.6D-E). An imprint for the intraparietal sulcus could be seen in four endocasts, in all four cases it can be seen perpendicular with the lunate sulcus (e.g. Fig. 5.6E). A pre-lunate sulcus was observed in two cases on the RH exclusively (Fig. 4.6B; D).

4.3.3 Occipital lobe:

Lunate sulcus impressions could be clearly identified on all the endocasts as a half-moon shaped impression that transects majority of the cerebral hemisphere indicating the rostral border of the occipital lobe (Fig 4.6). The inferior occipital sulcus was identified on more than half (LH = 4; RH = 5) of the endocasts on the inferior lateral extremities of the occipital lobe usually caudal to the lunate sulcus (Fig. 4.6F). Imprints of the lateral calcarine sulcus was identified on all the endocasts (LH = 5; RH = 6), in most cases as a horizontally orientated imprint on the occipital pole extending from the midline laterally (e.g. Fig. 3.6A).

4.3.4 Temporal lobe:

The superior temporal sulcus impression was identified on all six LH's and on five RH's, in most cases it could be identified parallel and inferior to the impression of the Sylvian fissure (e.g. Fig. 4.6C). The middle temporal sulcus was identified on more than half the endocasts on the LH and on three endocasts on the RH as showing a discontinuous pattern parallel and inferior to the superior temporal sulcus (Fig. 4.6B).

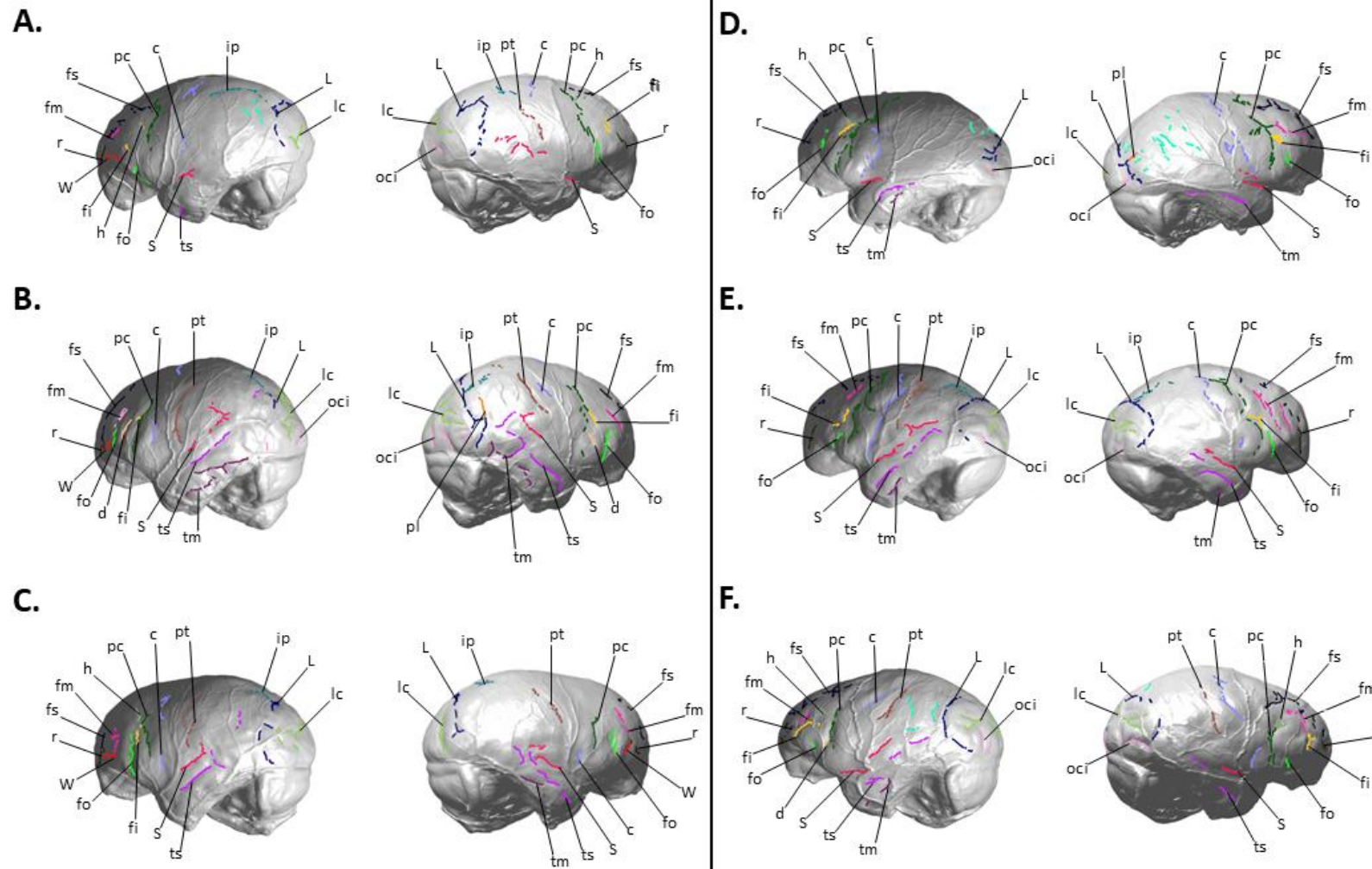


Figure 4.6: Sulcal pattern variation on six chimpanzee endocranial casts. A: Pan; B: Pan; C: Pan; D: Pan; E: Pan; F: Pan. The following sulci were identified: W=fronto-marginal sulcus; fo=fronto-orbital sulcus; r=sulcus rectus; fs=superior frontal sulcus; fm=middle frontal sulcus; fi=inferior frontal sulcus; d=diagonal sulcus; pc=precentral sulcus; h=horizontal ramus of pci; c=central sulcus; pt=postcentral sulcus; S=Sylvian fissure; ts=superior temporal sulcus; tm=middle temporal sulcus; ip=intraparietal sulcus; pl=pre-lunate sulci; L=lunate sulcus; oci=inferior occipital sulcus; lc=lateral calcarine sulcus

4.4 Probability Map

The following preliminary results are for the sulcal pattern variation on extant human endocasts only, which was presented in the form of a presentation at the annual meeting of the Anatomical Society of Southern Africa ([Appendix J](#))

The variation of sulcal imprints were documented up to two standard deviations (white) away from the mean (red – see Fig. 4.7).

The impressions of fronto-marginal sulci and fronto-orbital sulci (see Ono *et al.*, 1990) could be seen showing centralised distributions along the caudal margin of the frontal lobe (Fig. 4.8). Similar results can be seen for the superior frontal sulcus, which is evident to show a localised distribution more rostrally along the medial margin of the frontal lobe (Fig. 4.8). Furthermore, the middle frontal sulcus and the and the inferior frontal sulcus showed higher rates of variation compared to superior frontal sulcus (Fig. 4.8).

Scattered distributions could be seen for the precentral sulcus, central sulcus, postcentral sulcus and intraparietal sulcus, particularly on the LH (Fig. 4.9). The distribution of the right precentral sulcus clearly showed a localised distribution along the caudal area of the frontal lobe. Similarly, the vertically orientated left central sulcus showed a more centralised distribution located in the middle of the hemisphere just above the temporal lobe, marking the border between the frontal and parietal lobes (Fig. 4.9). The postcentral sulcus showed highly random distributions on the LH and a clear centralised distribution on the RH (Fig. 4.10). Additionally, the intraparietal sulcus showed two clusters of data however the most common area of identification was towards the caudal extremities of the parietal lobe (Fig. 4.10)

The occipital sulci from most rostral to caudal, the transverse occipital sulcus showed a centralised distribution on the superior lateral extremities of the occipital lobe with more variation of the transverse occipital sulcus being visible rostral on the LH (Fig. 4.10). Lateral/inferior occipital sulcus showed a mean distribution close to the inferior border of the occipital lobes, which showed to be situated more rostrally on the RH (Fig. 4.10). The lunate sulcus could be seen centralised in the middle of the occipital lobe directly caudal to the impression of the lambdoid suture (Fig. 4.10). Possible overlapping can be seen between the distributions of retro-calcarine- and lateral calcarine sulci which could be visualised horizontally distributed at the caudal pole on the LH (Fig. 4.11).

The Sylvian fissure showing a clear horizontal distribution on the lateral surface of the endocast separating the temporal lobe from the rest of the hemisphere. On the LH the Sylvian fissure is centralised rostrally compared to the longitudinal distribution on the RH (Fig. 4.12). The anterior horizontal ramus and the ascending ramus of the Sylvian fissure can be seen as centralised distributions on the inferior extremities of the frontal lobe. More extreme variations could be seen on the LH compared to the RH (Fig. 4.12). Additionally, the diagonal sulcus could be seen on the with significant overlapping with the ascending ramus as well as the precentral sulcus on both hemispheres (Fig. 4.12).

Finally, on the temporal lobes the superior temporal sulcus could be seen directly inferior to the impression of the Sylvian fissure showing a more centralised distribution towards the temporal pole. The superior temporal sulcus on the LH showed higher rates of variation towards the parietal lobe (Fig. 4.11). Similarly, the inferior temporal sulcus could be seen more centralised to the temporal poles with higher variation toward the occipital lobe on both hemispheres. Interestingly, the inferior temporal sulcus segmental distribution which is more evident on the LH compared to the RH (Fig. 4.8).



Animation of probability map showing the variation of sulcal imprints on the LH of extant human endocasts

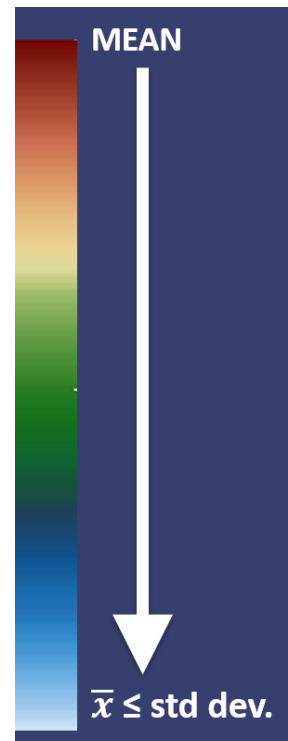


Figure 4.7: Key – dark red indicates mean (\bar{x}); light blue/white indicates variations up to two standard deviations (std dev.) from the mean

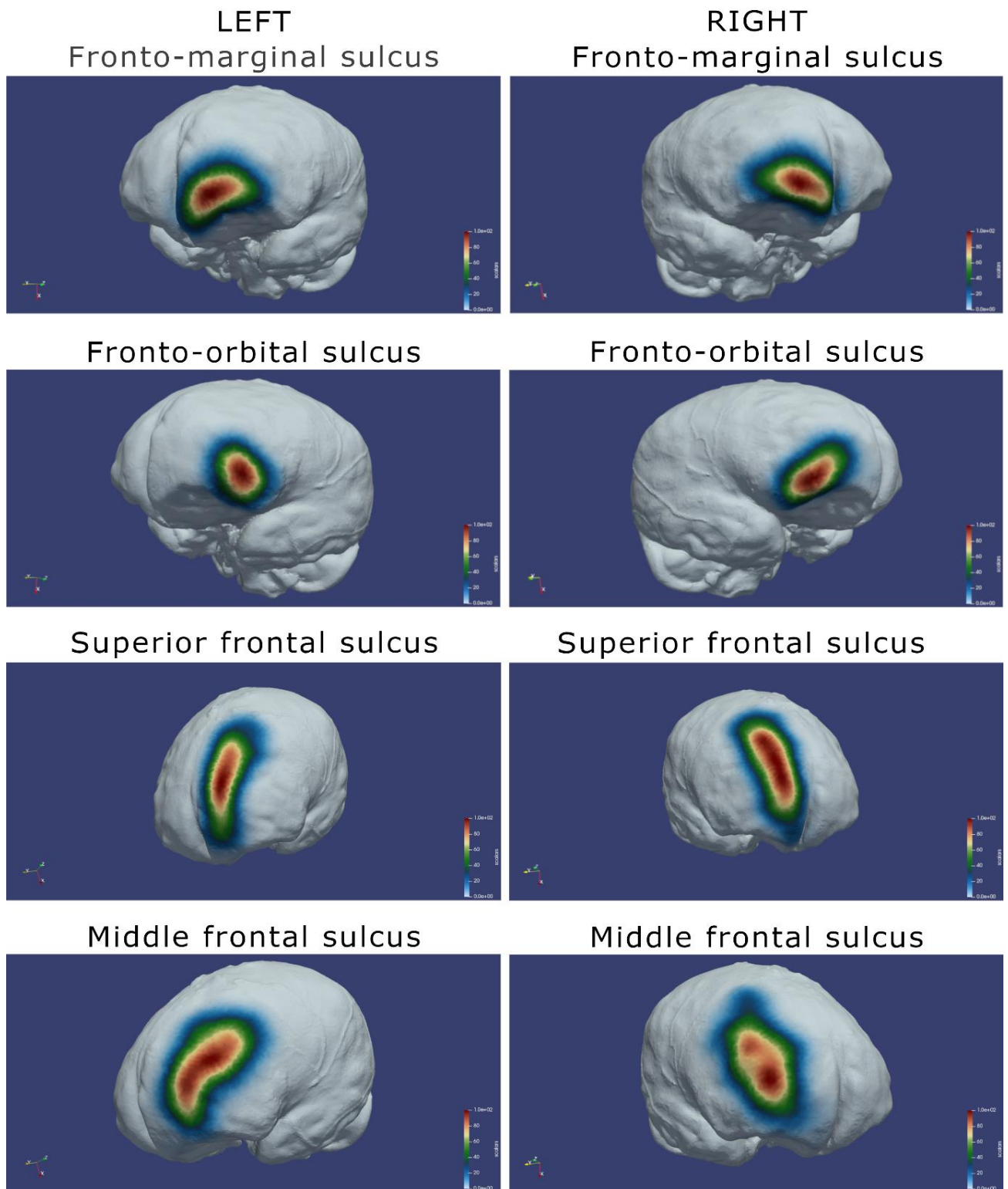


Figure 4.8: Probability map for the fronto-marginal-, fronto-orbital-, superior frontal- and middle frontal sulci on the left and right hemispheres

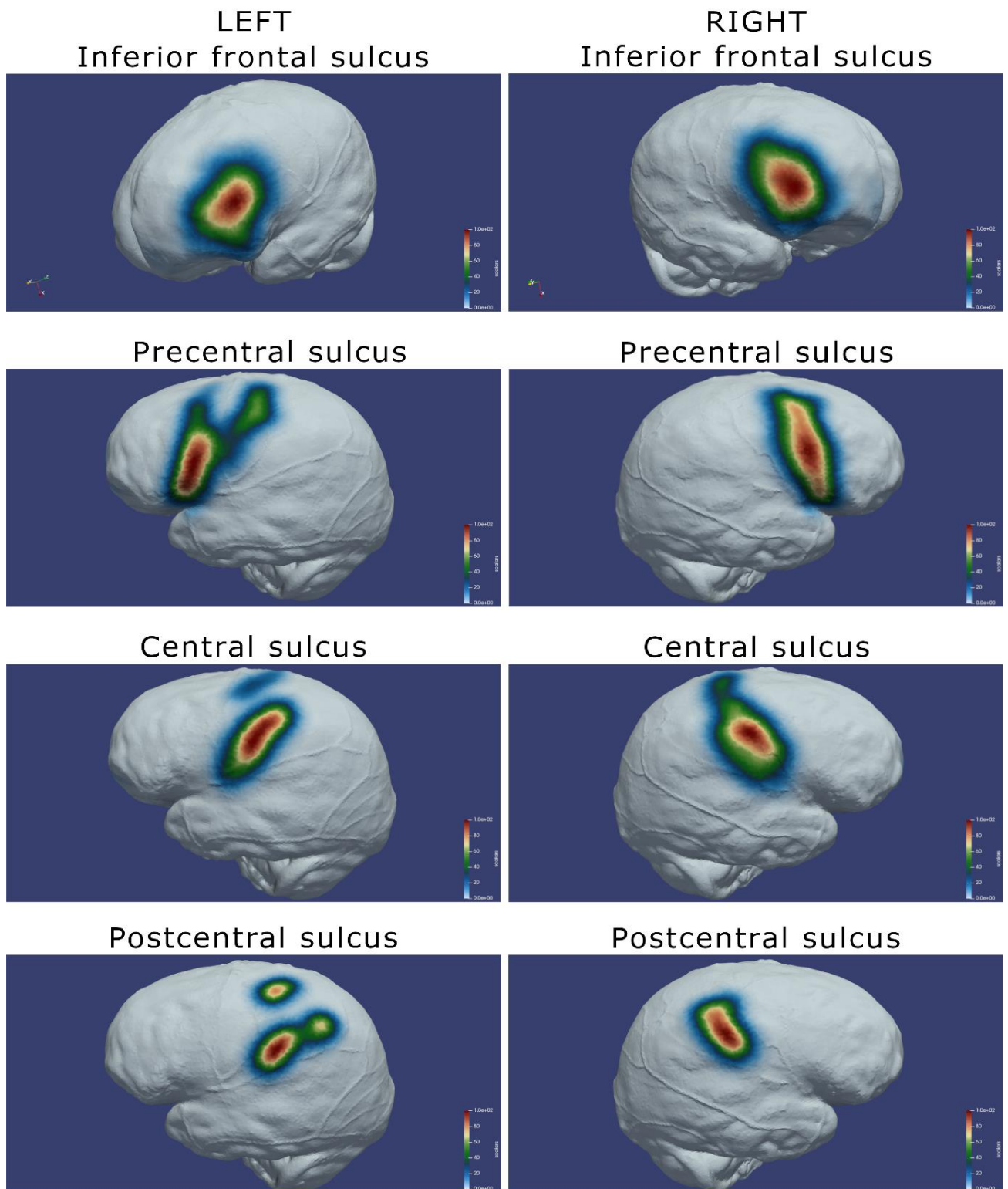


Figure 4.9: Probability map for the inferior frontal-, precentral-, central- and postcentral sulci on the left and right hemispheres

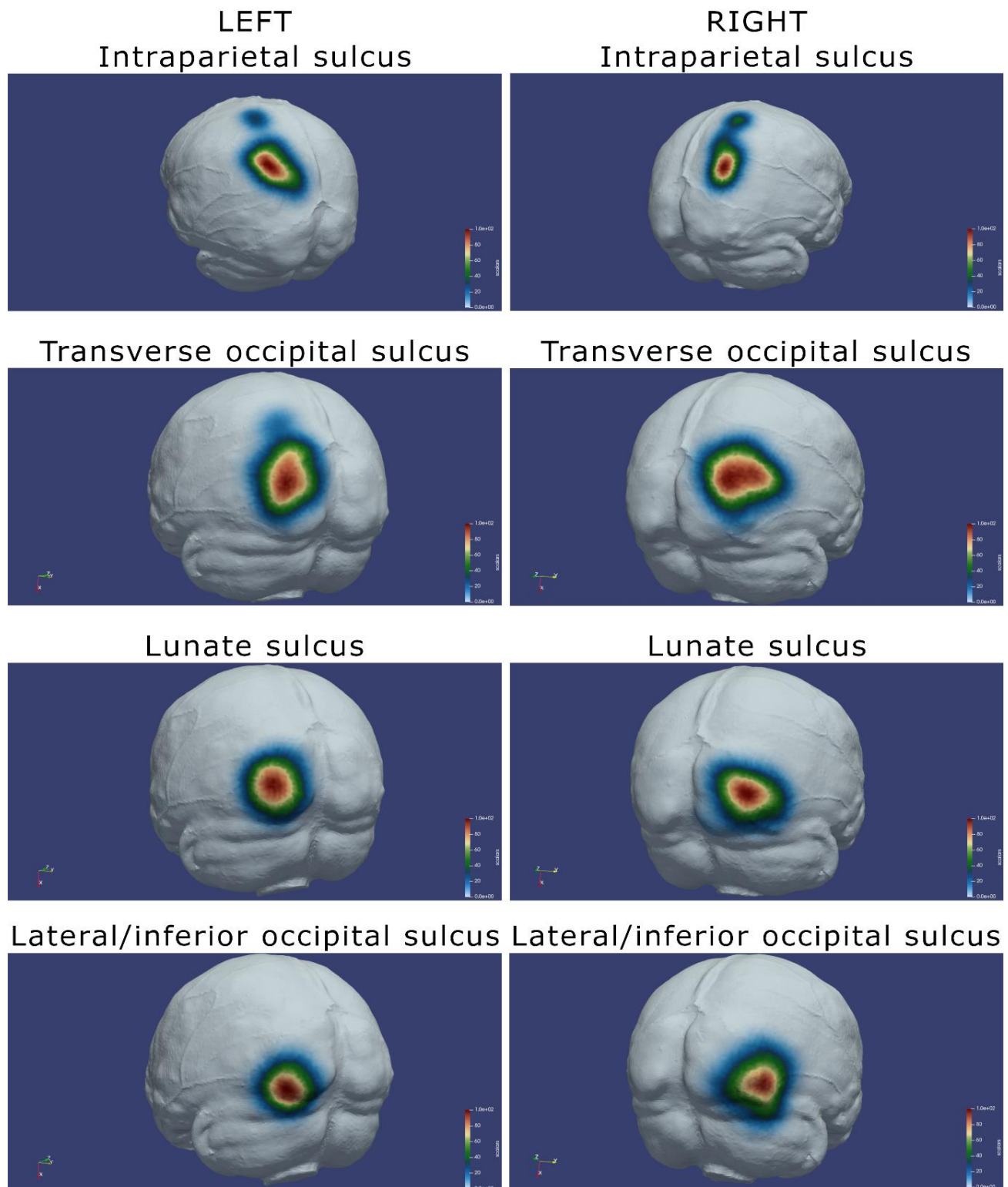


Figure 4.10: Probability map for the intraparietal-, transverse occipital-, lunate- and lateral/inferior occipital sulci on the left and right hemispheres

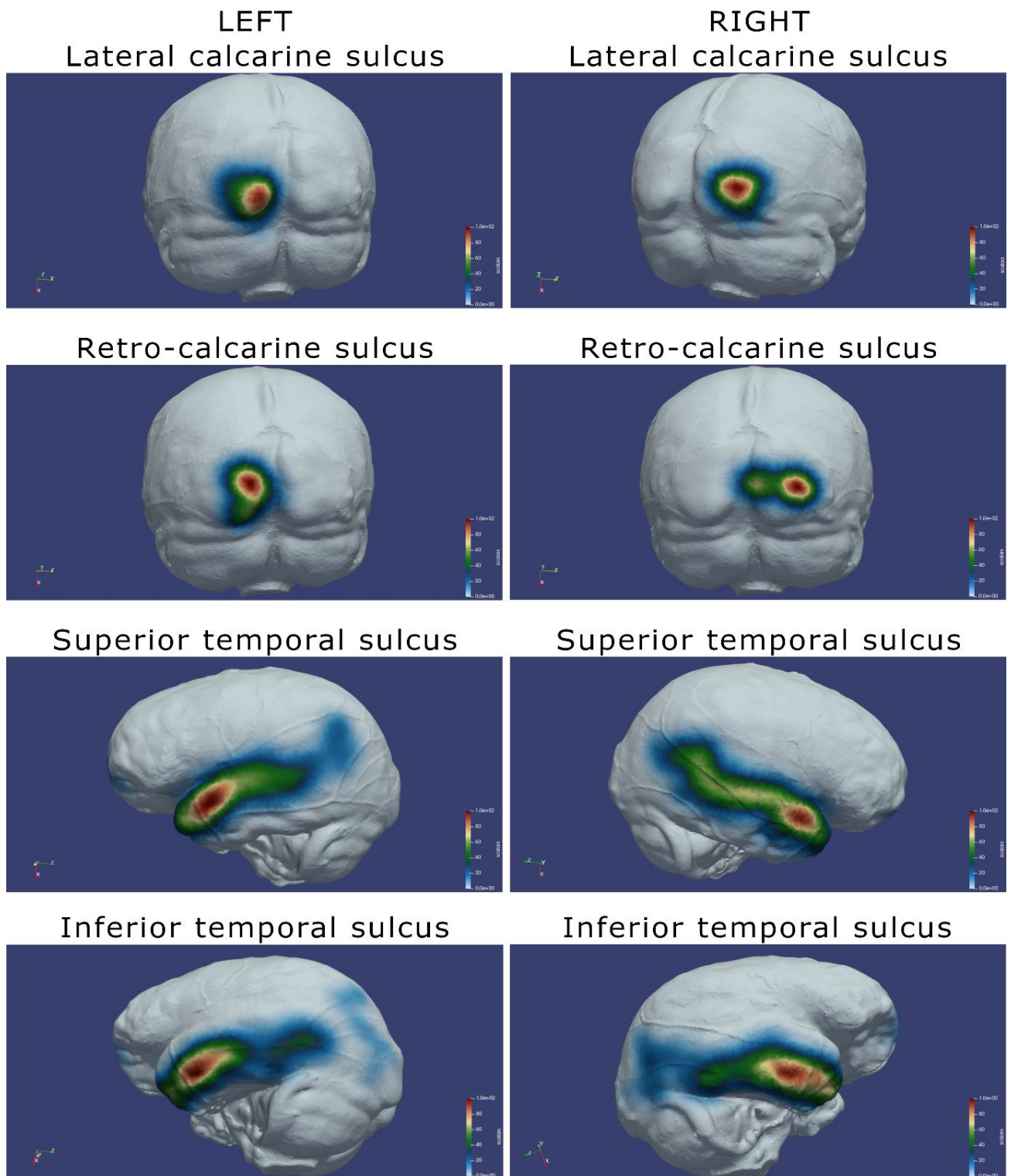


Figure 4.11: Probability map for the lateral calcarine-, retro-calcarine-, superior temporal- and inferior temporal sulci on the left and right hemispheres

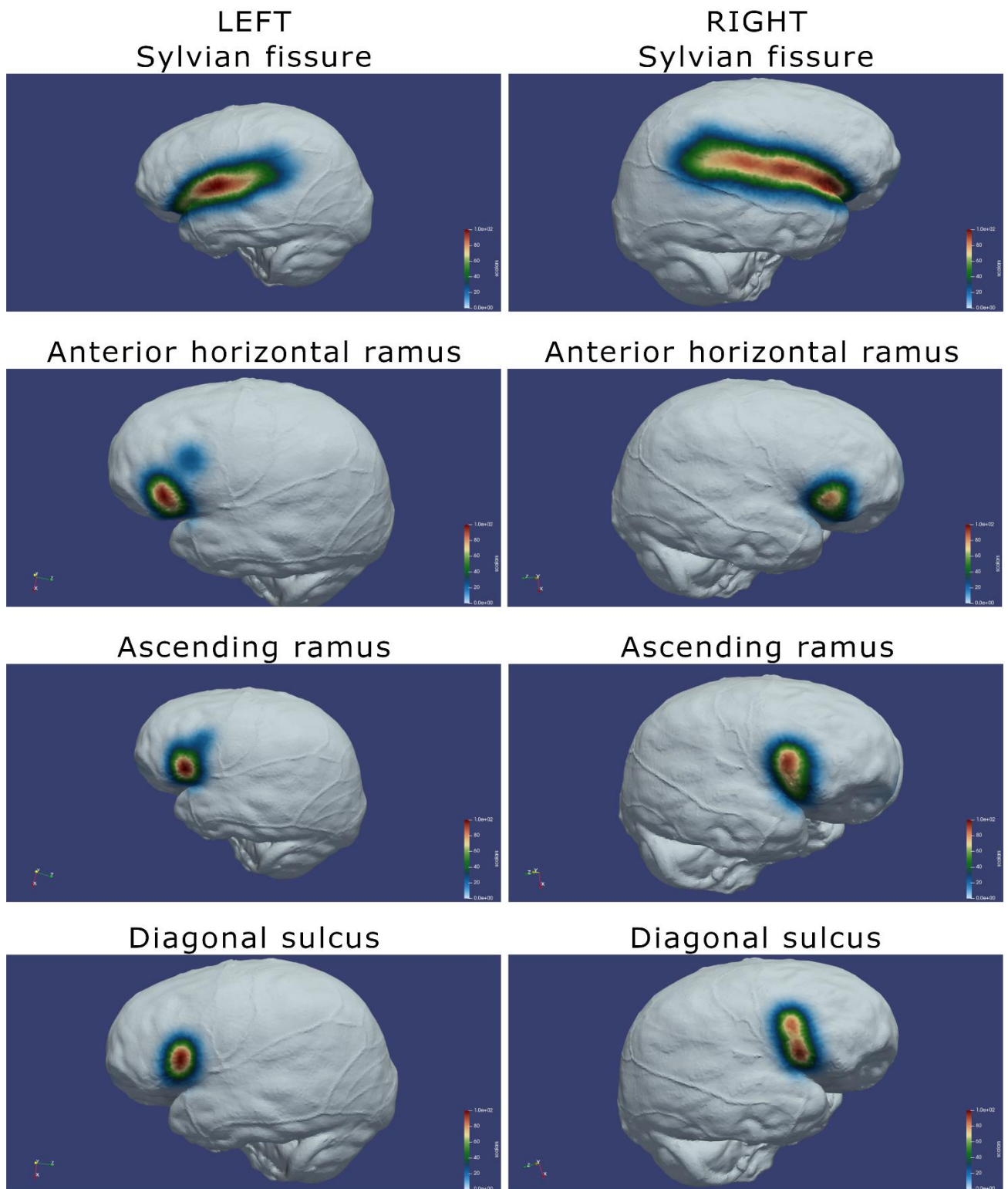


Figure 4.12: Probability map for the Sylvian fissure, anterior horizontal ramus, ascending ramus and diagonal sulcus on the left and right hemispheres

Chapter 5: Discussion

To the best of our knowledge this study provides the first description of sulcal imprint variation on extant human endocasts using a semiautomated probabilistic approach. Patterns of cortical sulci in formalin fixed brains from a South African collection were studied and documented to conceptualise the sulci that can be visualised on the superolateral cortical surface of the brain. Following this, high definition micro-CT and various software programs were utilised to explore cranial imprint pattern variation of cortical sulci in extant human- and *Pan* endocasts. Freely available software was used to automatically segment 58 human endocasts and 22 *Pan* endocasts to represent the surfaces of the cranium, an open source algorithm was used to detect topographical variations on the surface of the endocasts from which sulcal patterns were inferred using formalin-fixed brains and available literature as reference. After exclusions, the labelling of sulcal imprints were done using a custom script in Matlab to create a database (atlas) documenting sulcal imprints on 20 extant human endocasts (see de Jager *et al.*, 2019) and six *Pan* endocasts. Finally, by using the labelled data a probability map was created showing the variation of sulcal imprints on a common extant human endocast template (refer to section [4.4](#)).

For the purpose of this study, this discussion will focus on the detection and identification of sulcal pattern variations on extant human and *Pan* endocasts. These variations will be discussed in conjunction with findings from formalin-fixed brains and previous publications. Implications for future palaeoneurological studies will be discussed in conjunction with findings on a fossil endocast which was analysed based on data from this study (Beaudet *et al.*, 2018). As mentioned in section [4.2](#), a summary of this work on extant human endocasts was published in the Journal of Anatomy (de Jager *et al.*, 2019; [Appendix H](#)).

5.1 Sulcal pattern variation in extant human endocasts

Reliable identification of the orbital, temporal and frontal sulci and the Sylvian fissure could be performed in more than 80% of the endocasts. Descriptions of frequency and configuration of the orbital sulci, fronto-marginal, fronto-orbital, and lateral/inferior occipital

sulci are consistent with previous descriptions of brain sulci (Ono *et al.*, 1990; Chiavaras and Petrides, 2000; Iaria and Petrides, 2007). The most common configuration visualised for the orbital sulci were two anteriorly directed branches, a transverse sulcus and two posteriorly directed branches that typically form an “H” pattern, which directly correlates with patterns visualised on our local brain population and with descriptions from literature (Connolly, 1941; Chiavaras and Petrides, 2000). The fronto-marginal sulcus was identified as short horizontally orientated impressions extending laterally from the midline; possible overlapping was seen with superior frontal sulcus and middle frontal sulcus, correlating with findings from our formalin-fixed brain population as well as the findings from Ono *et al.*, (1990) and Connolly (1941) (Fig. 5.1). The fronto-orbital sulcus imprint was identified on the endocasts just anterior to “Broca’s cap³”, which could be easily misinterpreted, due the identification of this sulcus in humans being a rather controversial topic (see Connolly, 1950; Falk *et al.*, 2018; Petrides and Pandya, 2011).

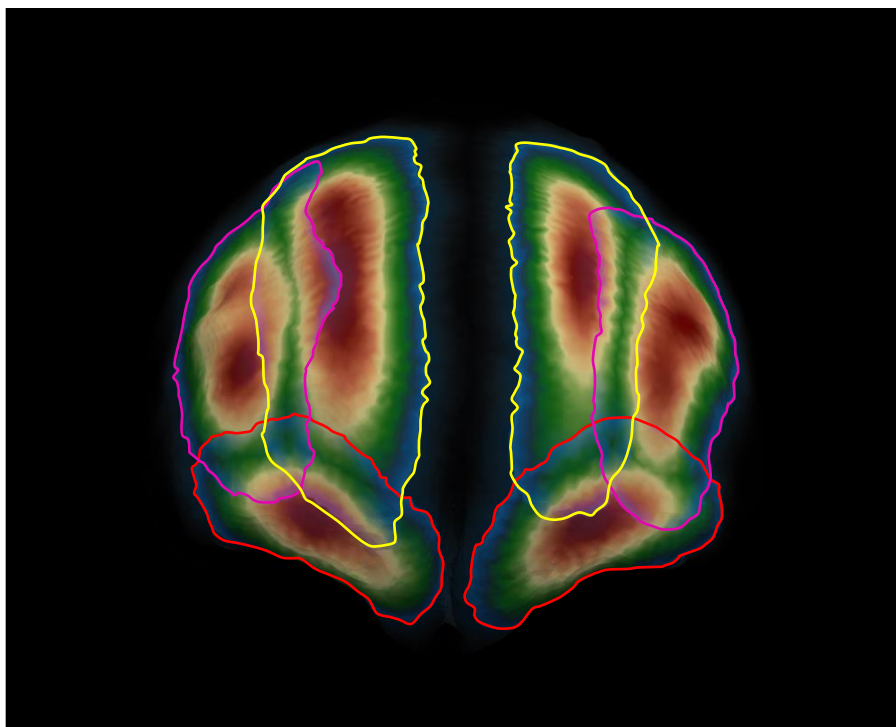


Figure 5.1: Illustration of the distribution of the imprints formed by superior frontal sulcus (yellow); the middle frontal sulcus (pink) and the fronto-marginal sulcus (red) on the frontal lobe

³ **Broca’s cap** (frontal cap, orbital cap) – the lateral and inferior protrusion of Broca’s area, which includes Brodmann’s areas 45, 47 and a portion of 44 (term originally introduced by Anthony, 1913; Holloway *et al.*, 2004; for discussion on homology see Falk, 2014)

The precentral sulcus could only be identified in fewer than half of the individuals, this was deemed due to distortion by the anterior bregmatic branch of the middle meningeal vessels (Bruner *et al.*, 2018). As a result, on the probability model created, the precentral sulcus on the left hemisphere shows high rates of variation, with possible overlapping with the central sulcus also observed (Fig 5.2). Despite this, it is evident from the probability map that the inferior part of precentral (pci) sulcus was identified in most cases, represented by the mean/mode observation in red (Fig. 5.2). Similarly, we could not reliably identify the postcentral sulcus and as a result this feature showed highly variable distribution on the probability map (Fig. 4.9 and 5.2), which may be due to the complex branching networks of blood vessels covering this area. CSF and blood vessels usually fill the main sulci that delineate functional areas and subsequently may not reproduce well on endocasts (Zollikofer and Ponce de León, 2013).

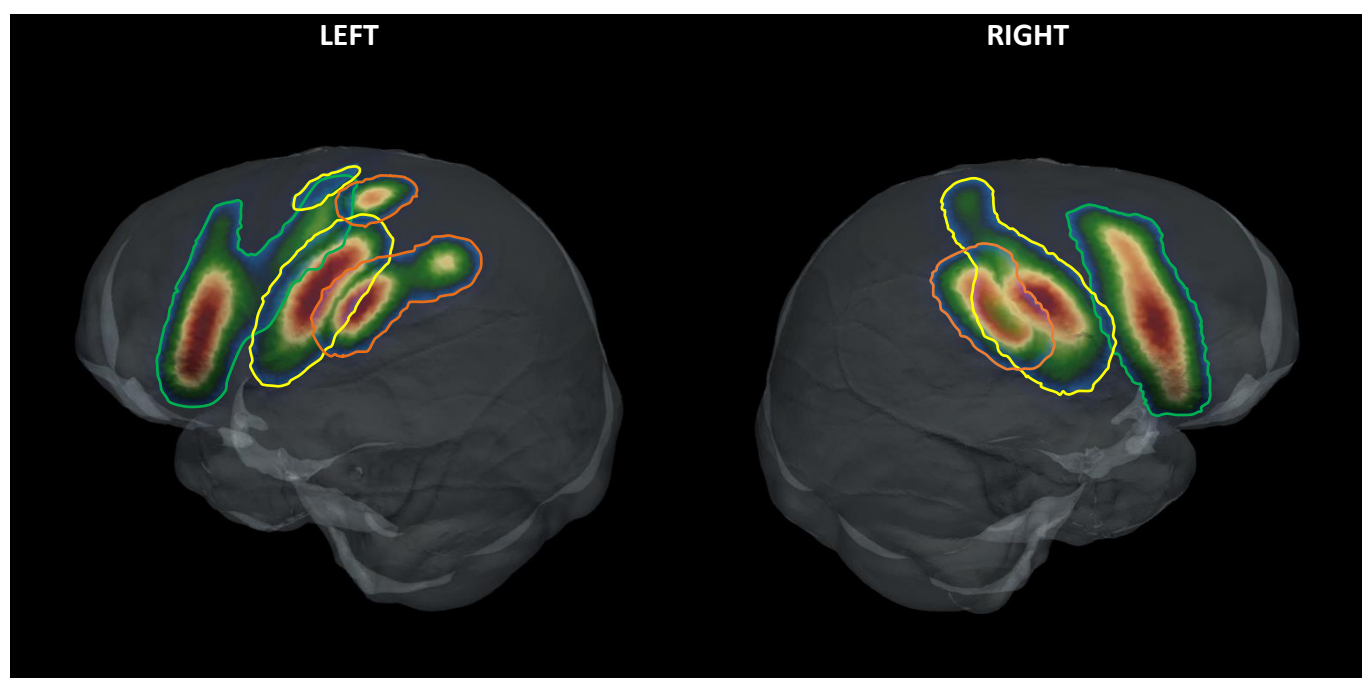


Figure 5.2: Illustration showing the probability map of the impressions formed by the precentral sulcus (green); the central sulcus (yellow) and the postcentral sulcus (orange) on the left and right hemispheres

Based on the information from the probability model, the transverse occipital sulcus can easily be misidentified on the endocasts due to the tendency of the intraparietal sulcus to terminate posteriorly close to the lambdoid suture, which frequently creates phantom markings on the endocast (Fig. 4.10). The impression created by the lambdoid suture on

cranial endocasts of extant humans does, however, prove useful in indicating the position of the superior extremities of the parietooccipital sulcus at the angle formed by the sagittal suture and the lambdoid suture, a landmark often used in neurosurgery (Ribas *et al.*, 2006).

Various morphological and functional differences have been noted between male and female brains (Holloway and de Lacoste, 1986; Zilles *et al.*, 2001; Liu *et al.*, 2010; Glezerman, 2016). While morphological differences may exist between male and female brains, these differences did not extend to sulcal patterns or sulcal imprint visibility on the endocasts selected for this study. These findings were further supported by observations on the formalin-fixed brain specimens examined in this study. Significant asymmetry was noted between the left and right hemispheres, when identifying the lateral calcarine sulcus, rhinal sulcus and collateral sulcus. The rhinal and collateral sulcal imprints are frequently misidentified on endocasts due to their vulnerability to distortion imposed by localised bony elements, which may also explain the perceived asymmetry. The lateral calcarine sulcus may also be asymmetrical (LHs= 55%; RHs= 20%), due to distortion occasionally created by overlay of the right dominant dural venous sinus groove (García-Tabernerero *et al.*, 2018). Evident on the probability map the lateral calcarine sulcus on the RH is clustered slightly more lateral than the LH, which may suggest that the dural venous sinuses are distorting the medially situated sulci (Fig. 4.11).

Minh and Hamada (2017) found that the expression of sulcal imprints on endocasts of Japanese macaques decreased with age, and other studies have proposed that no new brain expansion occurs in older individuals (Liu *et al.*, 2010), making it more difficult to identify sulcal imprints in crania of older individuals. We excluded age as a variable due to sample size constraints and therefore could not corroborate or reject the conclusions made by Liu *et al.* (2010).

5.2 Sulcal pattern impressions on the endocast of *Pan*

The modern *Pan* endocranial sulcal imprints have been described in meticulous detail by Le Gros Clark *et al.* (1936) who studied six cranial endocasts, and Connolly (1950) who described the sulcal imprints on one. No recent descriptions of sulcal imprint variation on *Pan* endocasts

are available. For that reason, we documented six cranial endocasts using our semi-automated approach. Sulci of the frontal lobe was consistently identified throughout all the samples. In particular, the fronto-orbital sulcus impression was continuously identified as a prominent impression throughout all the endocasts. It was found to typically extend over the orbital margin of the opercular part of the inferior frontal gyrus which is similar to the findings by Le Gros Clark *et al.* (1936). Additionally, main sulci such as the central sulcus, Sylvian fissure and superior temporal sulcus could clearly be identified in all six endocasts, which are known to be similar in the brains of all great apes (Connolly, 1950; Falk *et al.*, 2018).

Unlike the extant human endocast, the intraparietal sulcus was identified in more than half of the endocasts. Furthermore, the lunate sulcus was identified as a prominent trench transecting most of the lateral cerebral surface and marking the rostral border of the occipital lobe. Unlike the lack of imprints observed by Le Gross Clark *et al.* (1936), we observed highly variable patterns of the lateral calcarine sulcus caudal to the lunate sulcus, on the occipital pole (Fig. 4.6 and 5.3). Nonetheless, these results correlate with the findings presented in the literature (Le Gros Clark *et al.*, 1936; Connolly, 1950), and more recently in a study using MRI of chimpanzee brains (Falk *et al.*, 2018).

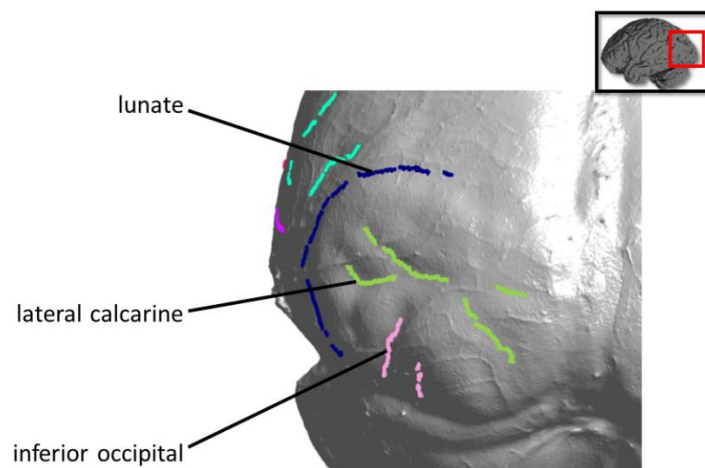


Figure 5.3: Illustration of sulci identified on the left occipital lobe of one *Pan* cranial endocast

5.3 Implications for palaeoneurological studies

We detected and identified sulci delimiting crucial cortical areas in the brain in more than one third of the human crania, including the lunate sulcus (80%) and the anterior horizontal (40%) and ascending rami (40%) of the Sylvian fissure, which are involved in critical debates in human palaeoneurology (Sherwood *et al.*, 2008; Falk, 2014). In particular, frontal sulci delimit crucial functional areas in neuroscience, including language, memory and motor functions (Petrides, 2005; Petrides and Pandya, 2011). The horizontal and the ascending rami of the Sylvian fissure, which we identified in nearly half (40%) of the human endocast samples on the LH, are suggested to have emerged with the genus *Homo*; Connolly (1950) suggested that with the expansion of the inferior frontal convolution the fronto-orbital sulcus in apes was displaced ventrally. In humans, the limiting sulcus of the insular lobe represents the homolog of the inferior part of the fronto-orbital sulcus in apes, which was identified directly anterior to “Broca’s cap” in all the *Pan* endocasts investigated. Although it has been theorised in earlier studies (Falk, 1983; Tobias, 1987; Carlson *et al.*, 2011), the recent discovery of a non-human hominin endocast with an intermediate pattern between the ape-like and human-like patterns suggests a more complex scenario (see discussion in Falk *et al.*, 2018). The middle frontal sulcus is also of particular interest in palaeoneurology due to its presence in non-human hominin endocasts and its relationship to the dorsolateral prefrontal cortex, which is involved in executive functions (Connolly, 1950; Van Essen, 2007; Falk, 2014). The rostral part of the middle frontal sulcus is considered as a homolog of the sulcus rectus in monkeys (see Fig. 5.4). In contrasting comparison, the caudal part is unique to humans, derived from the horizontal ramus of the inferior precentral sulcus, and is associated with the expansion of the frontal lobe (Eberstaller, 1890; Connolly, 1950; Falk, 2014). This segmented predisposition of middle frontal sulcus was visualised on the probability map, where the sulcal imprint variation of the middle frontal sulcus on the LH appears separated (Fig. 4.8).

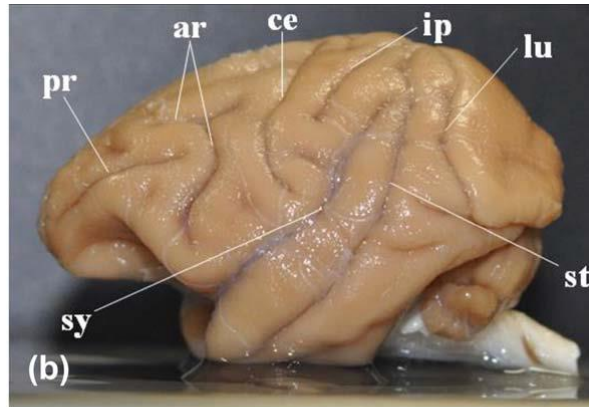


Figure 5.4: Photograph of macaque (*macaca fuscata*) brain from Minh and Hamada (2017); *pr*=principal sulcus/sulcus rectus; *ar*=arcuate sulcus/inferior precentral sulcus; *sy*=Sylvian fissure; *st*=superior temporal sulcus; *ce*=central sulcus; *ip*=intraparietal sulcus; *lu*=lunate sulcus

The lunate sulcus has been extensively described in association with human brains and is highly variable (Smith, 1903; Connolly, 1950; Ono *et al.*, 1990; Duvernoy *et al.*, 1999; Holloway *et al.*, 2004; Allen *et al.*, 2006). Although our sample size was small, the lunate sulcus was observed in 75% of the crania, which is more than the 62% in Ono *et al.* (1990) and 51.8% in Allen *et al.* (2006), but closely correlates with the 71% of this study's local formalin-fixed brain population. Larger endocast sample sizes (studied using similar methods or other populations) could shed more light on this matter. We observed the lunate sulcus anterior to the caudal pole of the occipital lobe as fragmented, vertically orientated impressions, usually depicting a curve. In one case we could visualize a lunate sulcus as described by Allen *et al.* (2006), traversing a substantial portion of the lateral surface of the posterior portion of the occipital lobe. As observations were made on endocasts and not cerebral surfaces, we are not able to comment on whether this impression is made by a 'true' or a composite lunate sulcus, however, humans generally do not have 'true' lunate sulci (Connolly, 1950; Allen *et al.*, 2006; Alves *et al.*, 2012). It is worth mentioning that throughout the formalin-fixed brain population, we identified the lunate sulcus depicting a possible composite configuration in at least 65% of hemispheres (see [Appendix G](#)). The impression of the lunate sulcus in one of the *Pan* endocasts showed a caudal placement when compared to the other *Pan* endocasts, which was hypothesized to be due to the superficial emergence of the first annectant gyrus of Gratiolet ([Fig. 4.6D](#)) (Connolly, 1950; Falk *et al.*, 2018). Nevertheless, our ability to automatically detect the lunate sulcus (or at the very least, fragments thereof) is important due to the past and ongoing debates regarding the homology of the lunate sulcus in humans

and apes, and the identification of the lunate sulcus in early hominin endocasts (Falk, 1980b; Holloway, 1981; Falk, 2014). The caudal placement of the lunate sulcus in hominins older than 2 million years may indicate early changes in the occipital lobes, probably related to the expansion of the parietal association cortex and a mosaic evolution of the cerebral areas (Falk, 1980b; Holloway, 1981; Holloway, 2001; Falk, 2014).

We were also able to identify the lateral calcarine sulcus more often than previously reported, namely in half of the crania, whereas Alves and co-authors (2012) identified a calcarine fissure on the superolateral surface of the brain at the level of the lateral occipital sulcus in 40% of brains. The size of the calcarine sulcus and its association with the primary visual cortex was recently discussed in Neanderthal brain endocasts, which revealed potential differences in visual capacity when compared to *Homo sapiens* (García-Taberner *et al.*, 2018).

5.4 The endocast of StW 573 (“Little Foot”)

Both atlases of extant human and *Pan* endocranial sulcal imprints were implemented in conjunction with adoption of a similar approach to developing them, was utilised to analyse the digital endocast of StW 573 (informally known as Little Foot), the results from which were published in the *Journal of Human Evolution* (Beaudet *et al.*, 2019; [Appendix K](#)). Little Foot is the most complete *Australopithecus* found in Member 2 of the Sterkfontein caves with a geological age of 3.67 million years (Granger *et al.*, 2015). The aim was to provide the first general description of Little Foot’s endocast, identify and comparatively describe the sulcal and vascular patterns, and finally, to discuss the significance thereof on human brain evolution. After the reconstruction and extraction of the endocast, the same approach was used to detect and identify imprints copied onto the endocast (refer to section [3.6.2](#)). This information was compared to ten other southern African *Australopithecus* and *Paranthropus* endocasts, in addition to the extant human and *Pan* endocasts. The authors found that the sulcal pattern visualised on the endocast shares resemblance to those of the other early hominin cranial endocasts as well as the patterns on the *Pan* endocranial cast, particularly on the inferior portion of the frontal lobe. The lunate sulcus was presumably identified just superior to the imprint of the sigmoid sinus, which is similar to identifications made on the *Pan* endocast (Beaudet *et al.*, 2019).

5.5 Limitations

Due to the exploratory design of this study, the following limitations need to be addressed to aid in conducting future studies. The formalin-fixed brains that were studied are part of a teaching collection for the training of medical students. Consequently, these specimens were only available for a limited time to document sulci, specifically from when the brain is removed from the embalmed body to when it is dissected by students. For this reason, a fully hands-on approach of studying these sulci was not entirely possible. Additionally, since this study focused on the patterns that are imprinted on the internal table of the crania collected by the medical school since 1943 (see L'Abbé *et al.*, 2005), there were no means of comparing our findings on the endocasts from a cranium, with the brain of the same individual. Subsequently, it was not possible to evaluate how accurate these identifications are, compared to the actual brain, thus observer bias of interpretation of the observations can be expected.

Due to this study being for degree purposes, time posed a substantial limitation that impacted on the sample size constraints for the endocasts documented (only twenty endocasts for the extant human population), which is acknowledged to have affected the precision of the probability map created. Finding *Pan* specimens available for research and in good condition was challenging. The future investigations on cranial endocasts will focus on increasing the sample size to improve the accuracy of the probability map, in conjunction with further optimisation of the software capabilities.

Cranial endocasts present with significant expanses of missing information, especially when studying cortical imprints on extant human endocasts. A similar concern was addressed by Neubauer *et al.* (2012) when studying **endocranial volume** in fossil specimens, whereby a thin-plate warping spline algorithm (Bookstein, 1997; Gunz *et al.*, 2005) was used to automatically reconstruct the endocast in question, based on a 'perfect' reference specimen. Since the possibility of acquiring a 'perfect' reference sample with all sulci flawlessly visible on the endocast is incredibly slim, the solution used by Neubauer *et al.* (2012) was not feasible for our current exploration of study, and therefore this limitation still requires address in future studies to prevent future hinderance of identifying the sulcal imprints automatically.

Chapter 6: Conclusion

This semi-automatic sulcal detection approach allowed the identification of sulci involved in executive functions and long-standing debates in palaeoanthropology. Despite the automatic sulci detection applied in this study, the identification of sulci by human observers may present a potential bias that should be taken into account when interpreting sulcal imprints in the fossil record. To address this, a parallel study is investigating the exact relationship of identifications on the endocasts of extant humans with the sulci on the same brain using scans from multiple imaging platforms of living individuals; the preliminary results for this study was presented as a poster in Bordeaux, France (Dumoncel *et al.*, 2018; [Appendix L](#)).

In conclusion, this atlas of extant human endocasts was used to construct a probability model documenting sulcal variation in extant humans, which will contribute to investigations pertaining to cortical evolution in the fossil record (Beaudet, 2017). Future research will increase the sample size to improve the accuracy of the probability map, and investigate methods to overcome missing data, and ultimately develop a protocol for the automatic recognition of cerebral imprints in fossil hominin endocasts (de Jager *et al.*, 2019).

Reference list

- Allen JS, Bruss J, Damasio H (2006) Looking for the lunate sulcus: A magnetic resonance imaging study in modern humans. *The Anatomical Record Part A: Discoveries in Molecular, Cellular, and Evolutionary Biology* 288A:867–876. doi: 10.1002/ar.a.20362
- Alves R V., Ribas GC, Párraga RG, de Oliveira E (2012) The occipital lobe convexity sulci and gyri. *Journal of Neurosurgery* 116:1014–1023. doi: 10.3171/2012.1.jns11978
- Amunts K, Jäncke L, Mohlberg H, Steinmetz H, Zilles K (2000) Interhemispheric asymmetry of the human motor cortex related to handedness and gender. *Neuropsychologia* 38:304–312. doi: 10.1016/S0028-3932(99)00075-5
- Amunts K, Schlaug G, Schleicher A, Steinmetz H, Dabringhaus A, Roland PE, Zilles K (1996) Asymmetry in the Human Motor Cortex and Handedness. *NeuroImage* 4:216–222. doi: 10.1006/nimg.1996.0073
- Anthony R (1913) L'encéphale de l'homme fossile de la Quina. *Bulletins et Mémoires de la Société d'anthropologie de Paris* 4:117–195. doi: 10.3406/bmsap.1913.8584
- Arnason U, Janke A (2002) Mitogenomic analyses of eutherian relationships. *Cytogenetic and Genome Research* 96:20–32. doi: 10.1159/000063023
- Beaudet A (2017) The Emergence of Language in the Hominin Lineage: Perspectives from Fossil Endocasts. *Frontiers in Human Neuroscience* 11:1–4. doi: 10.3389/fnhum.2017.00427
- Beaudet A, Clarke RJ, de Jager EJ, Bruxelles L, Carlson KJ, Crompton R, de Beer F, Dhaene J, Heaton JL, Jakata K, Jashashvili T, Kuman K, McClymont J, Pickering TR, Stratford D (2019) The endocast of StW 573 (“Little Foot”) and hominin brain evolution. *Journal of Human Evolution* 126:112–123. doi: 10.1016/j.jhevol.2018.11.009
- Beaudet A, Dumoncel J, de Beer F, Duployer B, Durrleman S, Gilissen E, Hoffman J, Tenailleau C, Thackeray JF, Braga J (2016a) Morphoarchitectural variation in South African fossil cercopithecoid endocasts. *Journal of Human Evolution* 101:65–78. doi: 10.1016/j.jhevol.2016.09.003
- Beaudet A, Dumoncel J, De Beer F, Durrleman S, Gilissen E, Hoffman J, Oettlé A, Subsol G, Thackeray JF, Braga J (2016b) Morphoarchitectural variation in the extant human endocast. In: *Journal of Human Evolution: 5 th Annual Meeting of the European Society for the study of Human Evolution, Madrid*; p 46.
- Beaudet A, Gilissen E (2018) Fossil Primate Endocasts: Perspectives from Advanced Imaging Techniques. In: Bruner E, Olgihara N, Tanebe H (eds) *Digital Endocasts: From Skulls to Brains*. Springer Japan, Tokyo; pp 47–58.
- Bookstein F (1997) *Morphometric tools for landmark data: geometry and biology*. Cambridge University Press, Cambridge.
- Bookstein FL (1989) Principal warps: thin-plate splines and the decomposition of deformations. *IEEE Transactions on Pattern Analysis and Machine Intelligence* 11:567–585. doi: 10.1109/34.24792

- Bosman MC (2008) *Neuroanatomy*, 2nd edn. University of Pretoria, Pretoria.
- Bruner E, Ogiwara N (2018) Surfin' endocasts: The good and the bad on brain form. *Palaeontologia Electronica* 21.1.1A:1–10. doi: 10.26879/805
- Bruner E, Ogiwara N, Tanabe HC (2018) *Digital Endocasts: from skulls to brains*, 1st edn. Springer Japan, Tokyo
- Carlson KJ, Stout D, Jashashvili T, de Ruiter DJ, Tafforeau P, Carlson K, Berger LR (2011) The Endocast of MH1, *Australopithecus sediba*. *Science* 333:1402–1407. doi: 10.1126/science.1203922
- Clarke RJ (2019) Excavation, reconstruction and taphonomy of the StW 573 *Australopithecus prometheus* skeleton from Sterkfontein Caves, South Africa. *Journal of Human Evolution* 127:41–53. doi: 10.1016/j.jhevol.2018.11.010
- Chiavaras MM, Petrides M (2000) Orbitofrontal sulci of the human and macaque monkey brain. *Journal of Comparative Neurology* 422:35–54. doi: 10.1002/(SICI)1096-9861(20000619)422:1<35::AID-CNE3>3.0.CO;2-E
- Cointepas Y, Mangin J-F, Garnero L, Poline J-B, Benali H (2001) BrainVISA: Software platform for visualization and analysis of multi-modality brain data. *NeuroImage* 13:98. doi: 10.1016/s1053-8119(01)91441-7
- Connolly CJ (1941) The fissural pattern in the brain of Negroes and Whites. The frontal lobes. *American Journal of Physical Anthropology* 28:133–165. doi: 10.1002/ajpa.1330280202
- Connolly CJ (1943) The fissural pattern in the brain of Negroes and Whites (continued). The occipital lobes. *American Journal of Physical Anthropology* 1:363–403. doi: 10.1002/ajpa.1330010410
- Connolly CJ (1950) *External morphology of the primate brain*. CC Thomas. Springfield, Illinois.
- Conroy GC, Vannier MW (1984) Noninvasive Three-Dimensional Computer Imaging of Matrix-Filled Fossil Skulls by High-Resolution Computed Tomography. *Science* 226:456–458. doi: 10.1126/science.226.4673.456
- Conroy G, Vannier M, Tobias P (1990) Endocranial features of *Australopithecus africanus* revealed by 2- and 3-D computed tomography. *Science* 247:838–841. doi: 10.1126/science.2305255
- Dart RA (1926) Taungs and its significance. *Natural History* 26:315–327.
- Deaner RO, Isler K, Burkart J, van Schaik C (2007) Overall Brain Size, and Not Encephalization Quotient, Best Predicts Cognitive Ability across Non-Human Primates. *Brain, Behavior and Evolution* 70:115–124. doi: 10.1159/000102973
- De Jager EJ, Van Schoor AN, Hoffman JW, Oettle AC, Fonta C, Beaudet A (2018) Sulcal pattern variation in extant human endocasts. In: *American Journal of Physical Anthropology: 87Th Annual Meeting of the American Association of Physical Anthropologists*, Austin; pp. 63-63.
- De Jager EJ, van Schoor AN, Hoffman JW, Oettlé AC, Fonta C, Mescam M, Risser L, Beaudet A (2019) Sulcal pattern variation in extant human endocasts. *Journal of Anatomy* 235:803–810. doi: 10.1111/joa.13030

- De Sousa A, Cunha E (2012) Hominins and the emergence of the modern human brain. *Progress in Brain Research* 195:293–322. doi: 10.1016/B978-0-444-53860-4.00014-3
- Dumoncel J, Subsol G, Durrleman S, Oettlé AC, Lockhat Z, Suleman FE, de Jager EJ, Beudet A (2018) A quantitative comparison of the brain and the inner surface of the cranium. In: 10ème Symposium de Morphométrie et Évolution des Formes. Bordeaux. (Unpublished)
- Duvernoy H, Bourguoin P, Cabanis E, Cattin F (1999) The human brain: functional anatomy, vascularization and serial sections with MRI. Springer. New York.
- Eberstaller O (1890) Das stirnhirn: ein beitrag zur anatomie der oberfläche des grosshirns. Urban and Schwarzenberg, Vienna and Leipzig.
- Evans AC, Collins DL, Neelin P, MacDonald D, Kamber M, Marett TS (1994) Three-dimensional correlative imaging: Applications in human brain mapping. In: Thatcher R, Hallet M, Zeffiro T, John E, Huerta M (eds) *Functional Neuroimaging: Technical Foundations*. Academic Press, San Diego; pp 145–162.
- Falk D (1980a) Comparative Study of the Endocranial Casts of New and Old World Monkeys. In: Ciochon RL, Chiarelli AB (eds) *Evolutionary Biology of the New World Monkeys and Continental Drift*. Springer, Boston, USA; pp. 275-292. doi:10.1007/978-1-4684-3764-5_13
- Falk D (1980b) A reanalysis of the South African australopithecine natural endocasts. *American Journal of Physical Anthropology* 53:525–539. doi: 10.1002/ajpa.1330530409
- Falk D (1983) Cerebral Cortices of East African Early Hominids. *Science*. 221:1072–1074.
- Falk D (1987) Hominid Paleoneurology. *Annual Review of Anthropology*, 16(1):13-28. doi:10.1146/annurev.an.16.100187.000305
- Falk D (2014) Interpreting sulci on hominin endocasts: old hypotheses and new findings. *Frontiers in Human Neuroscience* 8(May):1-11. doi:10.3389/fnhum.2014.00134
- Falk D, Hildebolt C, Smith K, Morwood MJ, Sutikna T, Brown P, Jatmiko, Saptomo EW, Brunnsden B, Prior F (2005) The Brain of LB1, *Homo floresiensis*. *Science* 308:242–245. doi: 10.1126/science.1109727
- Falk D, Redmond JC, Guyer J, Conroy GC, Recheis W, Weber GW, Seidler H (2000) Early hominid brain evolution: A new look at old endocasts. *Journal of Human Evolution* 38:695–717. doi: 10.1006/jhev.1999.0378
- Falk D, Zollikofer CPE, Ponce De León M, Semendeferi K, Alatorre Warren JL, Hopkins WD (2018) Identification of in vivo Sulci on the External Surface of Eight Adult Chimpanzee Brains: Implications for Interpreting Early Hominin Endocasts. *Brain, Behavior and Evolution* 91:45–58. doi: 10.1159/000487248
- Fiot J-B, Raguet H, Risser L, Cohen LD, Fripp J, Vialard F-X (2014) Longitudinal deformation models, spatial regularizations and learning strategies to quantify Alzheimer’s disease progression. *NeuroImage: Clinical* 4:718–729. doi: 10.1016/j.nicl.2014.02.002

- Garcia KE, Robinson EC, Alexopoulos D, Dierker DL, Glasser MF, Coalson TS, Ortinau CM, Rueckert D, Taber LA, Van Essen DC, Rogers CE, Smyser CD, Bayly P V. (2018) Dynamic patterns of cortical expansion during folding of the preterm human brain. *Proceedings of the National Academy of Sciences* 115:3156–3161. doi: 10.1073/pnas.1715451115
- García-Taberner A, Peña-Melián A, Rosas A (2018) Primary visual cortex in neandertals as revealed from the occipital remains from the El Sidrón site, with emphasis on the new SD-2300 specimen. *Journal of Anatomy* 233:33–45. doi: 10.1111/joa.12812
- Glasser MF, Coalson TS, Robinson EC, Hacker CD, Harwell J, Yacoub E, Ugurbil K, Andersson J, Beckmann CF, Jenkinson M, Smith SM, Van Essen DC (2016) A multi-modal parcellation of human cerebral cortex. *Nature* 536:171–178. doi: 10.1038/nature18933
- Glezerman M (2016) Yes, there is a female and a male brain: Morphology versus functionality. *Proceedings of the National Academy of Sciences* 113:E1971–E1971. doi: 10.1073/pnas.1524418113
- Granger DE, Gibbon RJ, Kuman K, Clarke RJ, Bruxelles L, Caffee MW (2015) New cosmogenic burial ages for Sterkfontein Member 2 Australopithecus and Member 5 Oldowan. *Nature* 522:85–88. doi: 10.1038/nature14268
- Gunz P, Mitteroecker P, Bookstein FL (2005) Semilandmarks in Three Dimensions. In: Slice D (ed) *Modern Morphometrics in Physical Anthropology*. Kluwer Academic Publishers-Plenum Publishers, New York; pp 73–98.
- Gunz P, Neubauer S, Maureille B, Hublin JJ (2010) Brain development after birth differs between Neanderthals and modern humans. *Current Biology* 20:921–922. doi: 10.1016/j.cub.2010.10.018
- Hershkovitz I, Greenwald C, Rothschild BM, Latimer B, Dutour O, Jellema LM, Wish-Baratz S (1999) Hyperostosis frontalis interna: An anthropological perspective. *American Journal of Physical Anthropology* 109:303–325. doi: 10.1002/(SICI)1096-8644(199907)109:3<303::AID-AJPA3>3.0.CO;2-I
- Hoffman JW, de Beer FCDE (2012) Characteristics of the Micro-Focus X-ray Tomography Facility (MIXRAD) at Necsa in South Africa. In: 18th World Conference on Nondestructive Testing, Durban.
- Holloway RL (1970) Australopithecine Endocast (Taung Specimen, 1924): A New Volume Determination. *Science* 168:966–968.
- Holloway RL (1978) The Relevance of Endocasts for Studying Primate Brain Evolution. In: Noback CR (ed) *Sensory Systems of Primates*. Springer, Boston; pp 181–200.
- Holloway RL (1980) Stereoplotting Hominid Brain Endocasts : Some Preliminary Results. In: Proceedings of the SPIE. pp 200–205.
- Holloway RL (1981) Revisiting the South African Taung australopithecine endocast: The position of the lunate sulcus as determined by the stereoplotting technique. *American Journal of Physical Anthropology* 56:43–58. doi: 10.1002/ajpa.1330560105

- Holloway RL (2001) Does allometry mask important brain structure residuals relevant to species-specific behavioral evolution? *Behavioral and Brain Sciences* 24:286–287. doi: 10.1017/S0140525X01303953
- Holloway RL (2008) The Human Brain Evolving: A Personal Retrospective. *Annual Review of Anthropology* 37:1–19. doi: 10.1146/annurev.anthro.37.081407.085211
- Holloway RL (2018) On the Making of Endocasts: The New and the Old in Paleoneurology. In: Bruner E, Ogiwara N, Tanabe HC (eds) *Digital Endocasts: From Skulls to Brains*. Springer, Tokyo; pp 1–8.
- Holloway RL, Broadfield DC, Yuan MS (2004) *The Human Fossil Record: Brain Endocasts, Volume 3*. John Wiley & Sons, Inc., New York.
- Holloway RL, de Lacoste MC (1986) Sexual dimorphism in the human corpus callosum: an extension and replication study. *Human neurobiology* 5:87–91.
- Holloway RL, Hurst SD, Garvin HM, Schoenemann PT, Vanti WB, Berger LR, Hawks J (2018) Endocast morphology of *Homo naledi* from the Dinaledi Chamber, South Africa. *Proceedings of the National Academy of Sciences* 115:5738–5743. doi: 10.1073/pnas.1720842115
- Iaria G, Petrides M (2007) Occipital sulci of the human brain: Variability and probability maps. *Journal of Comparative Neurology* 501:243–259. doi: 10.1002/cne.21254
- Jerison HJ (1973) *Evolution of the brain and intelligence*. Academic Press Inc., New York.
- Karcher H (1977) Riemannian center of mass and mollifier smoothing. *Communications on pure and applied mathematics* 30(5):509–541
- Keller SS, Roberts N, Hopkins W (2009) A Comparative Magnetic Resonance Imaging Study of the Anatomy, Variability, and Asymmetry of Broca's Area in the Human and Chimpanzee Brain. *Journal of Neuroscience* 29:14607–14616. doi: 10.1523/jneurosci.2892-09.2009
- L'Abbé EN, Loots M, Meiring JH (2005) The Pretoria Bone Collection: A modern South African skeletal sample. *HOMO- Journal of Comparative Human Biology* 56:197–205. doi: 10.1016/j.jchb.2004.10.004
- Langergraber KE, Prüfer K, Rowney C, Boesch C, Crockford C, Fawcett K, Inoue E, Inoue-Muruyama M, Mitani JC, Muller MN, Robbins MM, Schubert G, Stoinski TS, Viola B, Watts D, Wittig RM, Wrangham RW, Zuberbühler K, Pääbo S, Vigilant L (2012) Generation times in wild chimpanzees and gorillas suggest earlier divergence times in great ape and human evolution. *Proceedings of the National Academy of Sciences* 109:15716 LP – 15721. doi: 10.1073/pnas.1211740109
- Le Gros Clark WE (1971) *The antecedents of man; an introduction to the evolution of the primates*, 3rd edn. Quadrangle Books. Chicago.
- Le Gros Clark WE, Cooper DM, Zuckerman S (1936) The Endocranial Cast of the Chimpanzee. *The Journal of the Royal Anthropological Institute of Great Britain and Ireland* 66:249–268. doi: 10.2307/2844081

- Liu T, Wen W, Zhu W, Trollor J, Reppermund S, Crawford J, Jin JS, Luo S, Brodaty H, Sachdev P (2010) The effects of age and sex on cortical sulci in the elderly. *NeuroImage* 51:19–27. doi: 10.1016/j.neuroimage.2010.02.016
- Manger PR, Spocter MA, Patzke N (2013) The evolutions of large brain size in mammals: The “Over-700-gram club quartet.” *Brain, Behavior and Evolution* 82:68–78. doi: 10.1159/000352056
- McBrearty S, Jablonski NG (2005) First fossil chimpanzee. *Nature* 437:105–108. doi: 10.1038/nature04008
- Minh N Van, Hamada Y (2017) Age-related changes of sulcal imprints on the endocranium in the Japanese macaque (*Macaca fuscata*). *American Journal of Physical Anthropology* 163:285–294. doi: 10.1002/ajpa.23205
- Moorjani P, Amorim CEG, Arndt PF, Przeworski M (2016) Variation in the molecular clock of primates. *Proceedings of the National Academy of Sciences* 113:10607–10612. doi: 10.1073/pnas.1600374113
- Neubauer S (2014) Endocasts: Possibilities and limitations for the interpretation of human brain evolution. *Brain Behaviour and Evolution* 84(2):117–134. doi: 10.1159/000365276
- Neubauer S, Gunz P, Hublin J-J (2009) The pattern of endocranial ontogenetic shape changes in humans. *Journal of Anatomy* 215:240–255. doi: 10.1111/j.1469-7580.2009.01106.x
- Neubauer S, Gunz P, Weber GW, Hublin JJ (2012) Endocranial volume of *Australopithecus africanus*: New CT-based estimates and the effects of missing data and small sample size. *Journal of Human Evolution* 62:498–510. doi: 10.1016/j.jhevol.2012.01.005
- Ono M, Kubik S, Abernathy CD (1990) Atlas of the cerebral sulci. Thieme, Stuttgart.
- Paget J (1877) On a form of chronic inflammation of bones (osteitis deformans). *Medico-chirurgical transactions* 60:37.
- Perrot M, Rivière D, Mangin JF (2011) Cortical sulci recognition and spatial normalization. *Medical Image Analysis* 15:529–550. doi: 10.1016/j.media.2011.02.008
- Petrides M (2005) Lateral prefrontal cortex: Architectonic and functional organization. *Philosophical Transactions of the Royal Society B: Biological Sciences* 360:781–795. doi: 10.1098/rstb.2005.1631
- Petrides M, Orr SL, Sprug-Much T (2011): The intermediate frontal sulcus and its relation to the superior frontal sulcus. https://www.researchgate.net/publication/280529896_The_intermediate_frontal_sulcus_and_its_relation_to_the_superior_frontal_sulcus (accessed May 9, 2019).
- Petrides M, Pandya DN (2011) The Frontal Cortex. In: Mai J, Paxinos G (eds) *The Human Nervous System, Third edition*. Academic press, London; pp 988–1011.

- Prado-Martinez J, Sudmant PH, Kidd JM, Li H, Kelley JL, Lorente-Galdos B, Veeramah KR, Woerner AE, O'Connor TD, Santpere G, Cagan A, Theunert C, Casals F, Laayouni H, Munch K, Hobolth A, Halager AE, Malig M, Hernandez-Rodriguez J, Hernando-Herraez I, Prüfer K, Pybus M, Johnstone L, Lachmann M, Alkan C, Twigg D, Petit N, Baker C, Hormozdiari F, Fernandez-Callejo M, Dabad M, Wilson ML, Stevison L, Camprubí C, Carvalho T, Ruiz-Herrera A, Vives L, Mele M, Abello T, Kondova I, Bontrop RE, Pusey A, Lankester F, Kiyang JA, Bergl RA, Lonsdorf E, Myers S, Ventura M, Gagneux P, Comas D, Siegismund H, Blanc J, Agueda-Calpena L, Gut M, Fulton L, Tishkoff SA, Mullikin JC, Wilson RK, Gut IG, Gonder MK, Ryder OA, Hahn BH, Navarro A, Akey JM, Bertranpetit J, Reich D, Mailund T, Schierup MH, Hvilsom C, Andrés AM, Wall JD, Bustamante CD, Hammer MF, Eichler EE, Marques-Bonet T (2013) Great ape genetic diversity and population history. *Nature* 499:471–475. doi: 10.1038/nature12228
- Preacher KJ (2001) Calculation for the chi-square test: An interactive calculation tool for chi-square tests of goodness of fit and independence [Computer software]. Available from <http://quantpsy.org>.
- Ribas GC (2010) The cerebral sulci and gyri. *Neurosurgical Focus* 28:E2. doi: 10.3171/2009.11.focus09245
- Ribas GC, Yasuda A, Ribas EC, Nishikuni K, Rodrigues AJ (2006) Surgical anatomy of microneurosurgical sulcal key points. *Neurosurgery* 59:177–211. doi: 10.1227/01.NEU.0000240682.28616.b2
- Rivière, D., Geffroy, D., Denghien, I., Souedet, N., Cointepas, Y., 2009. BrainVISA: an extensible software environment for sharing multimodal neuroimaging data and processing tools. In: *Proceedings of the 15th HBM*.
- Sadler TW, Langman J (2012) Langman's medical embryology. Wolters Kluwer Health/Lippincott Williams & Wilkins, Philadelphia.
- Sanchez S, Ahlberg PE, Trinajstić KM, Mirone A, Tafforeau P (2012) Three-Dimensional Synchrotron Virtual Paleohistology: A New Insight into the World of Fossil Bone Microstructures. *Microscopy and Microanalysis* 18:1095–1105. doi: 10.1017/S1431927612001079
- Sherwood CC, Subiaul F, Zawidzki TW (2008) A natural history of the human mind: Tracing evolutionary changes in brain and cognition. *Journal of Anatomy* 212:426–454. doi: 10.1111/j.1469-7580.2008.00868.x
- Smith GE (1903) The so-called affenspalte in the human (Egyptian) brain. *Anatomischer Anzeiger* 24:74–83
- Specht M, Lebrun R, Zollikofer CPE (2007) Visualizing shape transformation between chimpanzee and human braincases. *The Visual Computer* 23:743–751. doi: 10.1007/s00371-007-0156-1
- Spoor F, Gunz P, Neubauer S, Stelzer S, Scott N, Kwakson A, Dean MC (2015) Reconstructed Homo habilis type OH 7 suggests deep-rooted species diversity in early Homo. *Nature* 519:83–86. doi: 10.1038/nature14224
- Spoor F, Jeffery N, Zonneveld F (2000) Using diagnostic radiology in human evolutionary studies. *Journal of Anatomy* 197:61–76. doi: 10.1017/S0021878299006408
- Standring S, Borley NR, Gray H (2008) Gray's anatomy : the anatomical basis of clinical practice, 40th edn. Churchill Livingstone/Elsevier. Edinburgh.

- Stiles J, Jernigan TL (2010) The basics of brain development. *Neuropsychology review* 20:327–48. doi: 10.1007/s11065-010-9148-4
- Subsol G, Gesquière G, Braga J, Thackeray F (2010) 3D automatic methods to segment virtual endocasts: state of the art and future directions. In: *American Journal of Physical Anthropology: 79th Annual Meeting of the American Association of Physical Anthropologists*, Albuquerque; pp. 226-227, Vol. 141 Issue S50.
- Tallinen T, Chung JY, Rousseau F, Girard N, Lefèvre J, Mahadevan L (2016) On the growth and form of cortical convolutions. *Nature Physics* 12:588–593. doi: 10.1038/nphys3632
- Tank PW (2012) Grant's dissector, 15th edn. Lippincott Williams & Wilkins, Philadelphia.
- Thirion J (1998) Image matching as a diffusion process: an analogy with Maxwell 's demons. *Medical Image Analysis* 2:243–260.
- Thompson PM, Toga AW (1997) Detection, visualization and animation of abnormal anatomic structure with a deformable probabilistic brain atlas based on random vector field transformations. *Medical Image Analysis* 1:271–294. doi: 10.1016/S1361-8415(97)85002-5
- Thompson P, Toga AW (1999) Anatomically Driven Strategies for High-Dimensional Brain Image Warping and Pathology Detection. In: Toga W (ed) *Brain Warping*. Academic Press, San Diego; pp 311–336.
- Thompson PM, Woods RP, Mega MS, Toga AW (2000) Mathematical/computational challenges in creating deformable and probabilistic atlases of the human brain. *Human Brain Mapping* 9:81–92. doi: 10.1002/(SICI)1097-0193(200002)9:2<81::AID-HBM3>3.0.CO;2-8
- Tobias P V. (1987) The brain of Homo habilis: A new level of organization in cerebral evolution. *Journal of Human Evolution* 16:741–761. doi: 10.1016/0047-2484(87)90022-4
- Tobias PV (2001) Re-creating ancient hominid virtual endocasts by CT-scanning. *Clinical Anatomy* 14:134–141. doi: 10.1002/1098-2353(200103)14:2<134::AID-CA1021>3.0.CO;2-F
- Toga AW, Thompson PM (2001) Maps of the brain. *Anatomical Record* 265:37–53. doi: 10.1002/ar.1057
- Toga AW, Thompson PM, Mori S, Amunts K, Zilles K (2006) Towards multimodal atlases of the human brain. *Nature Reviews Neuroscience* 7:952–966. doi: 10.1038/nrn2012
- Van Essen DC (2007) Cerebral Cortical Folding Patterns in Primates: Why They Vary and What They Signify. In: *Evolution of Nervous Systems*. Elsevier; pp 267–276.
- Vialard F-X, Risser L, Rueckert D, Cotter CJ (2012a) Diffeomorphic 3D Image Registration via Geodesic Shooting Using an Efficient Adjoint Calculation. *International Journal of Computer Vision* 97:229–241. doi: 10.1007/s11263-011-0481-8
- Vialard F-X, Risser L, Rueckert D, Holm DD (2012b) Diffeomorphic atlas estimation using geodesic shooting on volumetric images. *Annals of the British Machine Vision Association* 2012:1–12.
- Weber GW, Bookstein FL (2011) Virtual anthropology : a guide to a new interdisciplinary field, 1st edn. Springer-Verlag Wien.

- Wood B (2015) Wiley-Blackwell Student Dictionary of Human Evolution. John Wiley & Sons, West Sussex.
- Wood B, K. Boyle E (2016) Hominin taxic diversity: Fact or fantasy? *American Journal of Physical Anthropology* 159:S37–S78. doi: 10.1002/ajpa.22902
- Yoshizawa S, Belyaev A, Yokota H, Seidel H-P (2007) Fast and faithful geometric algorithm for detecting crest lines on meshes. In: Proceedings of Pacific Conference on Computer Graphics and Applications pp. 231-237. doi: 10.1109/PG.2007.26
- Yoshizawa S, Belyaev A, Yokota H, Seidel HP (2008) Fast, robust, and faithful methods for detecting crest lines on meshes. *Computer Aided Geometric Design* 25:545–560. doi: 10.1016/j.cagd.2008.06.008
- Zilles K, Kawashima R, Dabringhaus A, Fukuda H, Schormann T (2001) Hemispheric shape of European and Japanese brains: 3-D MRI analysis of intersubject variability, ethnical, and gender differences. *NeuroImage* 13:262–271. doi: 10.1006/nimg.2000.0688
- Zollikofer CPE, Ponce de León MS (2013) Pandora’s growing box: Inferring the evolution and development of hominin brains from endocasts. *Evolutionary Anthropology* 22:20–33. doi: 10.1002/evan.21333

Appendix A

The Research Ethics Committee, Faculty Health Sciences, University of Pretoria complies with ICH-GCP guidelines and has US Federal wide Assurance.

- FWA 00002567, Approved dd 22 May 2002 and Expires 03/20/2022.
- IRB 0000 2235 IORG0001762 Approved dd 22/04/2014 and Expires 03/14/2020.



UNIVERSITEIT VAN PRETORIA
UNIVERSITY OF PRETORIA
YUNIBESITHI YA PRETORIA

Faculty of Health Sciences Research Ethics Committee

31/08/2017

Approval Certificate New Application

Ethics Reference No: 339/2017

Title: Exploring an innovative method for the automatic recognition of cortical sulci in cranial endocasts

Dear Edwin de Jager

The **New Application** as supported by documents specified in your cover letter dated 21/08/2017 for your research received on the 22/07/2017, was approved by the Faculty of Health Sciences Research Ethics Committee on its quorate meeting of 30/08/2017.

Please note the following about your ethics approval:

- Ethics Approval is valid for 2 years
- Please remember to use your protocol number (**339/2017**) on any documents or correspondence with the Research Ethics Committee regarding your research.
- Please note that the Research Ethics Committee may ask further questions, seek additional information, require further modification, or monitor the conduct of your research.

Ethics approval is subject to the following:

- The ethics approval is conditional on the receipt of **6 monthly written Progress Reports**, and
- The ethics approval is conditional on the research being conducted as stipulated by the details of all documents submitted to the Committee. In the event that a further need arises to change who the investigators are, the methods or any other aspect, such changes must be submitted as an Amendment for approval by the Committee.

We wish you the best with your research.

Yours sincerely

Dr R Sommers; MBChB; MMed (Int); MPharMed, PhD

Deputy Chairperson of the Faculty of Health Sciences Research Ethics Committee, University of Pretoria

The Faculty of Health Sciences Research Ethics Committee complies with the SA National Act 61 of 2003 as it pertains to health research and the United States Code of Federal Regulations Title 45 and 46. This committee abides by the ethical norms and principles for research, established by the Declaration of Helsinki, the South African Medical Research Council Guidelines as well as the Guidelines for Ethical Research: Principles Structures and Processes, Second Edition 2015 (Department of Health).

☎ 012 356 3084 ✉ fhsethics@up.ac.za 🌐 <http://www.up.ac.za/healthethics>
✉ Private Bag X323, Arcadia, 0007 - Tswelopele Building, Level 4, Room 60, Gezina, Pretoria



Appendix B



06.06.2017

attestation

To whom it may concern,


Dr Amélie Beaudet from the University of the Witwatersrand has been given permission to access skeletal remains from the non-human primate collections which is housed in the Royal Museum for Central Africa, Tervuren (Belgium), for her postdoctoral research.

Sincerely Yours,

Dr. Emmanuel Gilissen
Curator of Mammals
Royal Museum for Central Africa
Department of African Zoology
Leuvensesteenweg 13
3080 Tervuren, Belgium
Phone: 32 (2) 769 56 22
Fax: 32 (2) 769 56 42
Email: Emmanuel.Gilissen@africamuseum.be






Appendix C	
QR code	
URL	https://drive.google.com/file/d/18EChH4BMcxGRHVw5k_7tDr8ZXLougRgs/view?usp=sharing

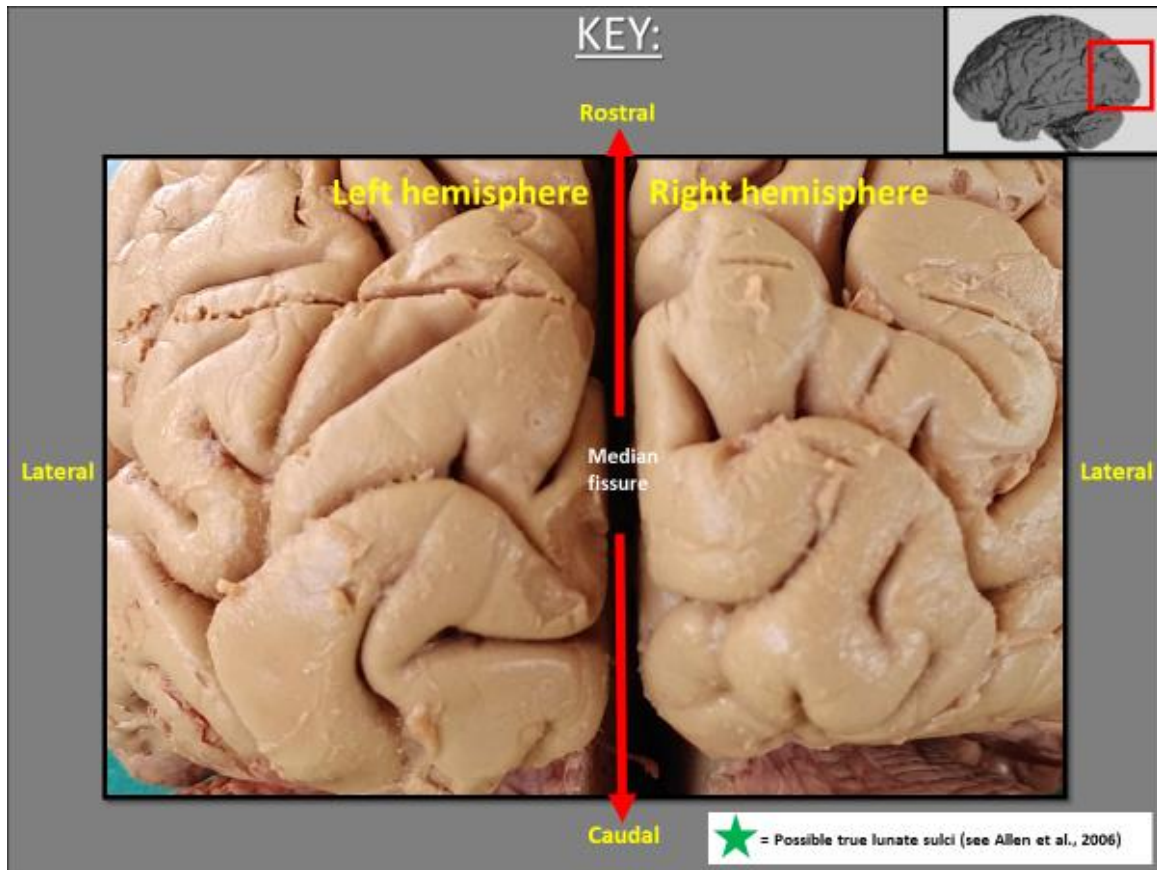
Appendix D	
QR code	
URL	https://drive.google.com/file/d/1pDrytbAzEPm7d9umnVPFotAZPmH6G7Cm/view?usp=sharing

Appendix E	
QR code	
URL	https://drive.google.com/file/d/1e3h30g_9l1Bdk5bJqNRkSaQ0EZ8fJ-g7/view?usp=sharing

Appendix F

1.	<p>Examples of orbital sulci variations (<i>o</i>) observed on the orbital surface: Photograph 1 - 3 → Clear depiction of the typical “H” configuration observed. Photograph 4 → More complex configurations of orbital sulci observed with some communication with fronto-marginal sulcus (<i>W</i>).</p>	
2.	<p>Some variations observed of fronto-marginal sulcus (<i>W</i>) and an example of the fronto-orbital sulcus identified (see Ono et al., 1990).</p>	
3.	<p>Examples of variations observed of superior frontal sulcus (<i>fs</i>), middle frontal sulcus (<i>fm</i>), inferior frontal sulcus (<i>fi</i>) and precentral sulcus (<i>pc</i>) on the frontal lobe. Additional sulci such as the fronto-marginal sulcus (<i>W</i>) and diagonal sulcus (<i>d</i>) are also mentioned.</p>	
4.	<p>Some relationships observed between the precentral sulcus (<i>pc</i>), central sulcus (<i>c</i>) and postcentral sulcus (<i>pt</i>). Additionally, examples of variations between <i>pt</i> and intraparietal sulcus (<i>ip</i>) are seen.</p>	
5.	<p>Examples of patterns of superior temporal sulcus (<i>ts</i>) and inferior temporal sulcus (<i>ti</i>) observed on the temporal lobe.</p>	
6.	<p>Examples of variations observed in the branches of the Sylvian fissure (<i>S</i>), specifically the sulcus and rami that border Broca’s motor speech area (Brodmann’s areas 44 & 45), which are namely the: diagonal sulcus (<i>d</i>), the ascending ramus (<i>ar</i>) and the horizontal ramus (<i>hr</i>).</p>	
7.	<p>Photograph 1 → Example of a possible true Lunate sulcus (<i>L</i>) observed. Photograph 2 & 3 → Examples of composite lunate sulci observed See Appendix G as well.</p>	


Appendix G




Abbreviations used:

Abbreviation	Sulcus
<i>L</i>	Lunate
<i>lc</i>	Lateral calcarine
<i>locs</i>	Lateral occipital
<i>oci</i>	Inferior occipital
<i>otr</i>	Transverse occipital
<i>pl</i>	Pre-lunate
<i>pm</i>	Paramedialis
<i>po</i>	Parietooccipital
<i>rc</i>	Retro-calcarine



Appendix H	
QR code	
URL	https://doi.org/10.1111/joa.13030

Appendix I	
QR code to poster	
URL to abstract	https://doi.org/10.1002/ajpa.23489

Appendix J

Quantifying the variation of sulcal patterns in extant human endocasts: a probabilistic approach

Edwin J. de Jager¹, Albert N. van Schoor¹, Jakobus W. Hoffman², Anna C. Oettlé^{1,3}, Caroline Fonta⁴, Muriel Mescam⁴, Laurent Risser⁵, Amélie Beaudet^{1,6}

¹Department of Anatomy, Faculty of Health Sciences, University of Pretoria, South Africa

²South African Nuclear Energy Corporation, Pelindaba, South Africa

³Department of Anatomy and Histology, Sefako Makgatho Health Sciences University, South Africa

⁴Centre de Recherche Cerveau et Cognition, Université de Toulouse, UPS, Toulouse, France

⁵Institute de mathématiques de Toulouse, Université de Toulouse, UPS, Toulouse, France

⁶School of Geography, Archaeology and Environmental Studies, University of the Witwatersrand, Johannesburg, South Africa

Our knowledge of human brain evolution primarily relies on the interpretation of palaeoneurological evidence. Endocasts (i.e., replica of the internal table of the bony brain case) constitute a proxy for reconstructing a timeline and mode of cerebral changes in the fossil record. The identification of cerebral imprints is critical for assessing the topographic extension and structural organisation of cortical areas. Describing these crucial landmarks in fossil endocasts is challenging due to the fragmentary nature of fossil specimens. Recent introduction of high-resolution imaging techniques in (palaeo)neurology offers new opportunities for tracking detailed endocranial neural characteristics. In this context, this study aims to provide an atlas that documents variation in the extant human endocranial sulcal patterns for subsequent use as a comparative platform for the study of the fossil record. Dry human crania from the Pretoria Bone Collection were scanned using micro-CT at Necsa, Pelindaba (South Africa). Endocasts were virtually extracted using Endex software. Sulci were automatically detected and manually labelled using a programme created with MATLAB. Finally, a probability map was created by projecting all the labelled sulci on an average endocast and calculating the average displacement of each identified sulcus. In providing an innovative, non-invasive, observer-independent method to investigate human endocranial structural organisation, our analytical protocol introduces a promising perspective for discussing long-standing questions in palaeoneurology.

Appendix K	
URL	https://doi.org/10.1016/j.jhevol.2018.11.009

Appendix L	
QR code	
URL	https://drive.google.com/file/d/1i4mctwFAfTsTXM8-cJcJWxsmUsVMQD1A/view?usp=sharing